ATLAS

Version 2.0 (December 2000)

ANALYSIS OF TIME-OF-FLIGHT DIFFRACTOMETER DATA FROM LIQUID AND AMORPHOUS SAMPLES

Incorporating the SANDALS survival guide

A.K.Soper, W.S.Howells, A.C.Hannon, J.Z.Turner and D.T.Bowron

CLRC ISIS Facility
Rutherford Appleton Laboratory
Chilton, Didcot, Oxon OX11 0QX

Tel: 01235-445543 (AKS)
01235-445680 (WSH)
01235-445358 (ACH)
01235-556397 (DTB)

TABLE OF CONTENTS

SECTION 5: APPENDICES

SECTION 1:

TIME-OF-FLIGHT DIFFRACTION

1.1 The time of flight neutron diffraction experiment

There are seven principle components to a time-of-flight diffraction experiment:
1. Production of neutrons in a target
2. Slowing down and thermalization of the neutrons in a moderator
3. Collimation of the neutrons into a beam
4. A sample to scatter the neutrons
5. A detector to measure the "diffraction" pattern of the scattered neutrons
6. A set of data acquisition electronics (DAE) to accumulate and store the data
7. A data analysis package

Normally the user is involved in providing the sample and performing the data analysis, the rest is provided as part of the neutron facility.

Production of neutrons at a spallation neutron source is achieved by accelerating bunches of protons to sufficiently high energies (typically 500-800MeV) that when they collide with a TARGET nucleus they produce highly excited nuclear states. These states either decay immediately or after a delay by throwing off nuclear particles such as neutrons, γ rays, neutrinos etc. The maximum energy of neutrons produced in this way corresponds to the energy of the impinging proton beam, and if the target is uranium, up to 30 neutrons per proton can be produced. Other non-fissioning targets such as tantalum or tungsten produce about half the number of neutrons. The so-called "prompt" neutrons are the ones used for time-of-flight analysis while the "delayed" neutrons form a low level background in the diffractometer which is independent of time. This background in general must be corrected for as it can be sample dependent. Normally the delayed fraction is on the order of a few tenths of a percent of the prompt neutrons, but in cases where an enriched booster target is installed, such as at the Argonne National Laboratory in the US, this fraction can be higher.

The proton beam is pulsed so that a pulse of neutrons less than 1μs wide is produced in the target. These neutrons are however not useful as they typically have energies 10^9 times too high for diffraction effects to be seen. These neutrons are therefore slowed down in a MODERATOR that scatters the neutrons many times before they escape. Light atoms such as found in hydrogenous materials (e.g. methane or water) are used for the moderator since the energy transferred in a collision is greatest when the two particles have the same mass. Up to a point, the thicker the moderator, the slower the neutrons become, but the process is self limiting, because as well as slowing the neutrons down, the moderator has the effect of broadening the initial very narrow pulse significantly. Moderators are therefore designed to compromise between the production of slow neutrons and the requirements for reasonably narrow neutron pulses. In comparison with a nuclear reactor, the spallation target would be regarded as under-moderated. The target-moderator assembly is surrounded by neutron reflecting material, usually beryllium, to enhance the neutron production and pulse shape.

Figures 1.1 and 1.2 show a typical neutron spectrum from the methane moderator at ISIS, plotted as a function of energy and time-of-flight respectively. Two regions in the spectrum can be identified, the epithermal region where the intensity varies as 1/E, or 1/t, respectively, and a Maxwellian "hump" which occurs when the neutrons in the moderator reach a temperature close to that of the moderator. The neutron spectrum is therefore described by two functions which are added together using a joining function [2].

TITLE : Neutron spectrum v. energy
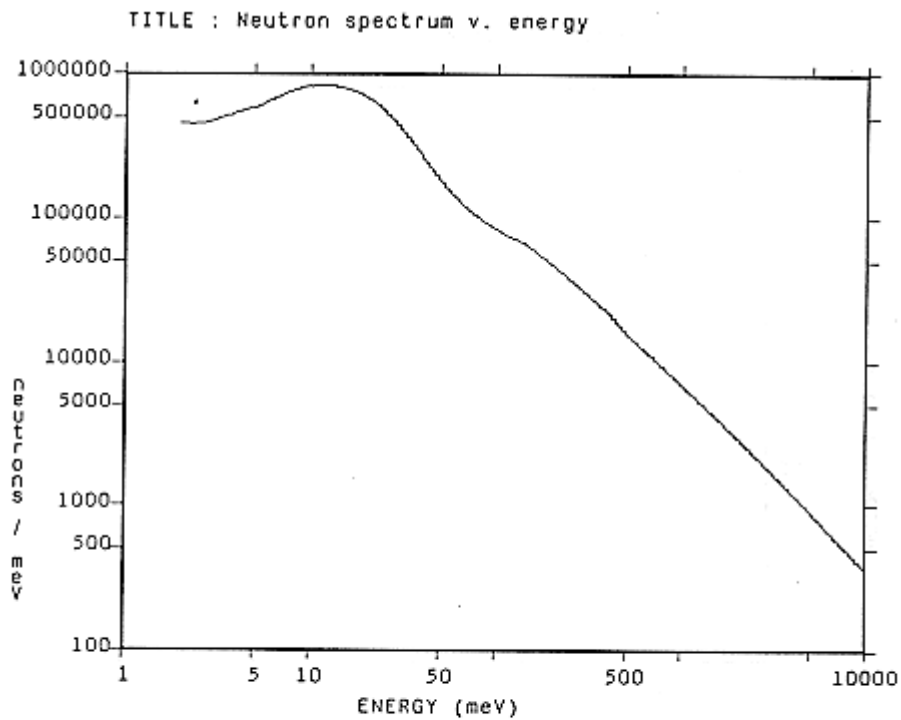
Figure 1.1 Time-of-Flight neutron spectrum as a function of energy.
Note the log scales used in the graph

TITLE : Neutron spectrum v. wavelength
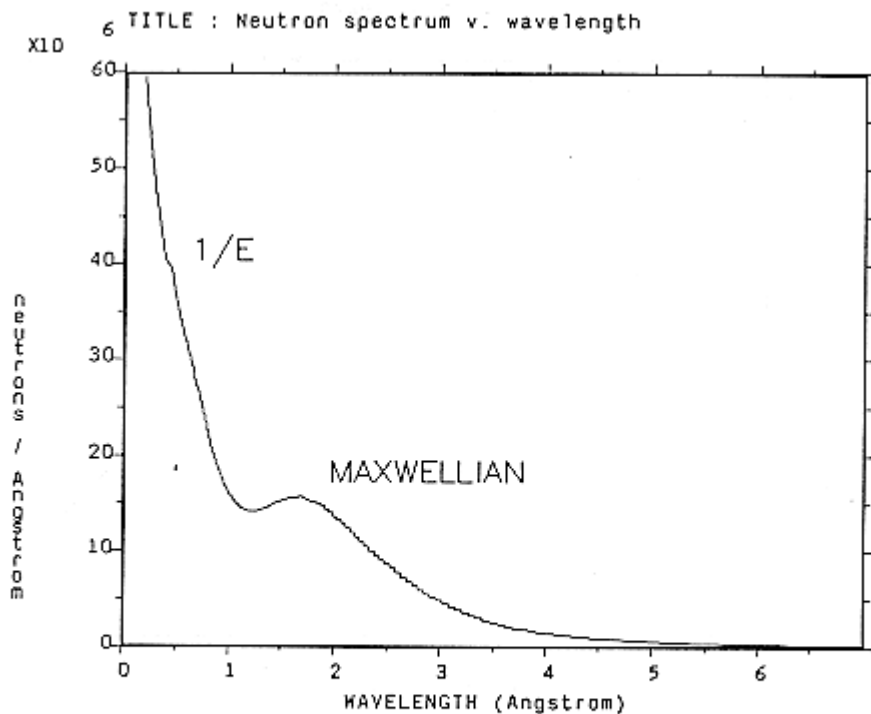
Figure 1.2 Time-of-Flight spectrum as a function of neutron wavelength

The Maxwellian region is described by the function:

$$\Phi_{max}(E) = J\ (E/T^2)\ \exp(-E/T) \qquad\qquad 1.1.1$$

while the slowing down epithermal region is represented by

$$\Phi_{epi}(E) = \Phi_0\ /\ E^A \qquad\qquad 1.1.2$$

These two functions are combined by means of an empirical switch function, $\Delta(E)$:

$$\Phi(E) = \Phi_{max}(E) + \Delta(E)\Phi_{epi}(E) \qquad\qquad 1.1.3$$

where

$$\Delta(E) = [1 + \exp\{W_1/\sqrt{E} - W_2\}]^{-1} \qquad\qquad 1.1.4$$

In these equations J is the integrated Maxwellian intensity, T is the effective temperature of the Maxwellian in energy units, Φ_0 is the differential flux at 1eV, A is a leakage parameter and W_1, W_2 are two parameters which define the switch function. Table 1.1 lists the values of these constants for the methane and ambient moderators at ISIS.

	CH$_4$	Ambient H$_2$O
Epithermal[*]		
Φ_0 (at 750MeV)	2.7	3.5
[10^{10} n (eVsr100cm$^2\mu$As)$^{-1}$]		
A	0.92	0.9
Maxwellian		
J	5.7	14.7
[10^{10} n (sr100cm$^2\mu$As)$^{-1}$]		
T (eV)	0.011	0.033
Joining function		
W_1 (eV)$^{\frac{1}{2}}$	1.7	4.0
W_2	7.0	10.6

Table 1.1 ISIS moderator constants

[*]N.B. The above numbers for the Φ_0 refer to 750MeV proton energy. The 100cm^2 refers to the area of the moderator normally viewed.

The neutrons emerge from the moderator in all directions and so to be useful for diffraction they must be COLLIMATED. An essential difference between TOF and reactor diffraction is that there is no monochromator for the TOF experiment which means the full spectrum of neutron energies, from 800 MeV downwards, is incident on the sample. It then follows that materials like cadmium and gadolinium which might be used in a reactor situation are useless in the TOF case, and may even be detrimental because of the high energy γ's produced by neutron capture in those materials. Instead boron, which has a 1/v capture cross section over a wide energy range, is the primary component, with large amounts of iron and hydrogen (the

latter usually in the form of wax or resin) to provide the basic scattering cross section. Since the final scattered intensities are small compared to the incident beam intensity, and because it is essential to provide a radiation free environment for people working near the diffractometer, the TOF collimator is a massive construction. At ISIS the collimator plus shielding measures typically ≈1.5m square. Figure 1.3 shows a diagram of the prototype SANDALS collimator. This collimator is surrounded on all four sides by about 0.4m of iron, and a further 0.3m borated wax outside the iron.
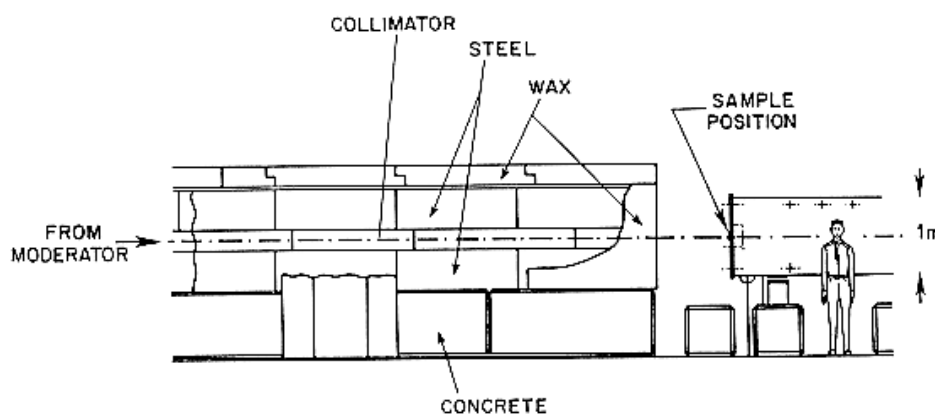
Figure 1.3 Diagram of the prototype SANDALS collimator illustrating the bulkiness of neutron shielding at ISIS.

The collimator defines a NEUTRON BEAM at the sample position. This must be sufficiently well collimated to give adequate angular resolution for the type of experiment being undertaken, but large enough to give an acceptable count rate. Crystalline powder experiments generally need high resolution in order to discriminate effectively between adjacent Bragg reflections and also to determine the sample contribution to the shape of individual reflections. However, because Bragg reflections are so sharp in count rate is rarely a severe constraint, unless special effects are being determined, such as the change in structure as a function of time. In contrast for liquids and amorphous materials the structure factor consists of a few broad peaks which merge together continuously. Detailed analysis of these requires absolute measurements. In many cases, particularly those that involve measuring changes in structure as a function of pressure, temperature or isotope, count rate can be of paramount importance because of the intrinsic weakness of the signal. Increases in resolution can only be used if a count rate appropriate to the resolution is available.

The sample is normally held in a CONTAINER: in addition if the temperature is to be different from ambient then a FURNACE is required to go above room temperature, and a CCR (Closed Cycle Refrigerator), for temperature down to 20K, or HELIUM CRYOSTAT, for temperatures down to 4.2K is required. Somewhat lower temperatures can be achieved by pumping on the helium in the cryostat.

For accurate structure factor measurements the mounting and containment of the sample can be crucial since the diffractometer is sensitive to small positioning offsets on the order of 1mm. This sensitivity arises from the small variations in final flight path and scattering angle which can occur from one sample to another if each sample is not placed in exactly the same position as its predecessor. One solutions to this difficulty which is applicable if the sample will not be under pressure is to use a flat plate sample can with an area larger than the beam area. This largely avoids the positioning problems. In general however cylindrical cans must be used for pressure or furnace experiments and so it is essential to ensure that if cylindrical cans are used to sample positioning is accurate to 0.1mm.

Ideally the container should be made of a purely incoherent scattering material (vanadium or titanium-zirconium are the closest to this ideal), otherwise the Bragg reflections from the container can be hard to subtract completely. This problem arises because the front and back of the sample container correspond to slightly different times of flight. Thus when the container measured empty and then filled with sample, the neutron attenuation by the sample causes the Bragg peaks from the front of the container to be attenuated preferentially compared to those from the rear, causing an apparent shift in the position of the peaks in time. Once again the ideal of an incoherent container may be hard to meet if a particularly corrosive sample requires a special material for containment. Fortunately titanium-zirconium allow is suitable for many pressure vessels.

The next diffractometer component, the DETECTOR, adopts one of two forms. It is usually a gas proportional counter, with ^{3}He gas the primary neutron absorber, but at ISIS there has been considerable development work on neutron scintillator detectors. If all goes well the use should not have to be particularly concerned about which kind of detector he is using, although he should be aware of its efficiency and deadtime. The reasons for choosing scintillator detectors for liquids and amorphous materials centre on their much lower cost compared to ^{3}He tubes, and on the fact that they can be made at least twice as efficient as the He tube. In this way the epithermal part of the neutron can be used more effectively.

The primary object of the DATA ACQUISITION ELECTRONICS, DAE, is to record each neutron event and give it a label corresponding to the number of the detector in which it occurred and to the time of arrival at the detector. The clock which measures this time of arrival is started by an electronic pulse which is generated when a burst of protons hits the target. At ISIS this occurs 50 times a second. Once the label is generated, a word of memory corresponding to the label is incremented. In this way a histogram of events is built up. The experiment is controlled by a FRONT END MINIcomputer (FEM) which is a computer to store, manipulate and display the data.

After transmission through the sample the neutrons and other particles are absorbed in a BEAM STOP, which again at ISIS is of a massive construction, as it must absorb all potentially dangerous particles which come down the beam line. In fact different pulsed neutron sources have adopted different modes of operation. At the HARWELL linac and at the LANSCE facility at Los Alamos, parts of the facility are inaccessible while the beam is on, in order to protect experimenters from radiation exposure. At ISIS on the other hand the shielding is sufficiently comprehensive that even when running at full power the background radiation levels are certainly low enough for people to remain near the diffractometers for extended periods.

The time of arrival, t_0, of a neutron at the detector is given by its "TIME-OF-FLIGHT", TOF, which is the time (in μs) taken by the neutron to travel 1m, multiplied by the total flight path in metres. Several useful relationships can be written down between the neutron's time of flight TOF (μsm^{-1}), velocity v (ms^{-1}), wavelength λ (Å), wavevector ($Å^{-1}$) and energy E (in meV). Thus

v (ms^{-1}) = 10^6 / TOF (μsm^{-1})
λ (Å) = 0.0039562 TOF = 0.0039562 t_0 (μs)/L (m)
t_0 (μs) = 252.77L
k ($Å^{-1}$) = 2π/λ = 1588.2 / TOF
e (meV) = 81.807/λ^2 1.1.5

Using these relationships we can write down the incident flux distribution as a function of wave vector or wavelength in terms of the energy distribution:

$\Phi(\lambda) = \Phi(E)(\delta E/\delta\lambda) = 2\Phi(E)(E/\lambda)$

$\Phi(k) = \Phi(E)(\delta E/\delta k) = 2\Phi(E)(E/k)$ etc.   1.1.6

Note that since in the epithermal region $\Phi(E) \approx \Phi_0/E$, then

$\Phi(\lambda) = 2\Phi_0/\lambda$, $\Phi(k) = 2\Phi_0/k$ etc.

An important characteristic of any diffractometer is its resolving power: it is the Q-RESOLUTION which makes the primary distinction between a powder diffractometer, where there are many sharp peaks close together and so requires high resolution, and the liquids and amorphous diffractometer where the peaks are broader. Merge together continuously and hence requires relatively low resolution. For liquids and amorphous materials diffractions, irrespective of whether it is constant wavelenth or time-of-flight diffraction, the scattered intensity, which is proportional to the structure factor S(Q) (see section 1.2), is measured versus the momentum transfer, $\hbar Q$, where for elastic scattering

$Q = 4\pi \sin\theta/\lambda$ 1.1.7

2θ is the scattering angle and λ the neutron wavelength. In the case of TOF, λ is measured by time-of-flight with θ held constant. In that case we see that the resolution, ΔQ, has two components:

$\Delta Q = (\delta Q/\delta\theta)\Delta\theta + (\delta Q/\delta\lambda)\Delta\lambda$

   $= Q[(\cot\theta\Delta\theta) + \Delta\lambda/\lambda]$ 1.1.8

The wavelength uncertainty, Δλ/λ, arises from the intrinsic pulse width of the incident neutron beam and from the flight path uncertainty to the detector, ΔL/L, where L is the total flight path from moderator to the detector. A more detailed account of contributions to the resolutions function is given in Appendix A. We note that for a given TOF channel the width of the pulse, Δv, as a function of neutron velocity, v, is proportional to v, i.e. Δv/v = Δλ/λ = constant. Similarly since for a given time channel

$\lambda \sim 1/L(m)$

it will be seen that the flight path uncertainty also gives rise to a wavelength uncertainty such that $\Delta\lambda/\lambda = \Delta L/L$ = constant as a function of t_0. Hence we see from (1.1.3) that the resolution $\Delta Q/Q$ is roughly a constant as a function of TOF for a given scattering angle.

Further details about the effects of resolution are given in Appendix A. The count rane on a diffractometer is denoted by its "count rate number" or "C number" (see Appendix B for details). Table 1.2 lists the resolution and C-numbers for SANDALS.

<div align="center">Table 1.3 Some specifications for SANDALS</div>

Moderator:	Methane 100K
Incident Flight Path:	11m
Beam Cross Section:	Circular
Maximum Beam Aperture:	32mm diameter
Final Flight Path:	0.75m-4.0m
Detectors:	Zinc sulphide sandwich detectors
	200 (high) x 10 (wide) x 20 (deep) mm
	30% efficient at 10eV

Range in 2θ	Detector solid angle	High resolution		Low Resolution	
(Deg)	(sr)	Resolution $\Delta Q/Q$ (%)	C-number $(Q=10\text{Å}^{-1})$	Resolution $\Delta Q/Q$ (%)	C-number $(Q=10\text{Å}^{-1})$
3-11	0.039	11-2	0.3	16-4	6
11-21	0.110	2	1.4	4-3	32
19-31	0.202	1.5	3.5	3	76
29-41	0.275	1.3	5.5	2.5	120

1.2 Overview of diffraction theory

The quantity that is sought it a diffraction experiment on any crystalline or disordered material is the STRUCTURE FACTOR, S(Q) :

$$S(\mathbf{Q}) = 1 + \rho\int dr\, (g(\mathbf{r}) - 1)\, \exp(i\mathbf{Q}.\mathbf{r}) \qquad 1.2.1$$

Where ρ is the number density of atoms in the material, $g(\mathbf{r})$ the pair correlation function at position $\mathbf{r}$ given an atom at the origin, and $\mathbf{Q}$ is the reciprocal lattice vector or wave vector transfer in the diffraction experiment. The integral is taken over the entire volume of the sample. $S(\mathbf{Q})/\rho$ is to be regarded as the density of points in reciprocal space, just as $\rho g(\mathbf{r})$ the density of points in real space.

From the definition of the structure factor (1.2.1) although different from the normal definition for structure factor used in crystallography, is nonetheless valid irrespective of whether the sample is a single crystal, polycrystalline, amorphous or fluid. However for

powders, glasses and fluids an immediate simplification is possible because $S(\mathbf{Q})$ and $g(\mathbf{r})$ then depend only on the magnitude of $\mathbf{Q}$ and $\mathbf{r}$ respectively and not on their directions. (This statement is equivalent to saying that the points in reciprocal space and real space are distributed uniformly into shells of radius Q and r respectively). Hence the integral over spherical polar angular coordinates in (1.2.1) can be performed directly:

$$S(Q) = 1 + 4\pi\rho/Q \int_0^\infty r\,dr\,(g(r)-1)\sin(Qr) \qquad\qquad 1.2.2$$

Although this is now a one-dimensional integral, it is important to bear in mind that the diffraction experiment probes $S(Q)$ in three dimensions.

For a multicomponent system there is a term like (1.2.1) or (1.2.2) for each distinct pair of atomic types α,β; all the partial structure factors $S_{\alpha\beta}(Q)$, are summed together in the TOTAL STRUCTURE FACTOR with weights proportional to the product of the scattering lengths for each atomic type:

$$F(Q) = \sum_\alpha c_\alpha \langle b_\alpha^2\rangle + \sum_{\alpha,\beta} c_\alpha\langle b_\alpha\rangle c_\beta\langle b_\beta\rangle (S_{\alpha\beta}(Q)-1) \qquad\qquad 1.2.3$$

Where c_α is the atomic fraction, b_α is the scattering length, or element α and the bars indicate averages over the spin and isotope states of each element, assuming of course that these are not correlated with position. The first term in (1.2.3) is called the "SELF" or "SINGLE ATOM" scattering, whilst the second is called the "INTERFERENCE" or "DISTINCT" scattering, because it contains the basic structural information on atomic positions.

The quantity measured in a neutron diffraction experiment is strictly NOT the structure factor, but the DIFFERENTIAL CROSS-SECTION, which is defined as

$$\frac{d\sigma}{d\Omega}(\lambda,2\theta) = \frac{\left(\begin{array}{c}\text{Number of neutrons scattered per unit time}\\ \text{into the small solid angle } d\Omega \text{ at angle } 2\theta\end{array}\right)}{N\,\Phi(\lambda)\,d\Omega} \qquad\qquad 1.2.4$$

Where N is the number of atoms (or scattering units if such a definition is more convenient) in the sample, and $\Phi(\lambda)$ is the incident neutron flux at wavelength λ. As for the structure factor the differential cross-section can be split into "self" and "distinct" terms:

$$d\sigma/d\Omega = d\sigma/d\Omega_S + d\sigma/d\Omega_D \qquad\qquad 1.2.5$$

In the absence of any corrections for attenuation, multiple scattering and inelasticity effects, the differential cross section is equal to the total structure factor, $F(Q)$. This is known as the STATIC APPROXIMATION. In particulat the self and distinct parts are defined as:

$$d\sigma/d\Omega_S = \sum_\alpha c_\alpha \langle b_\alpha^2\rangle$$

And

$$d\sigma/d\Omega_D = \sum_{\alpha,\beta} c_\alpha \langle b_\alpha\rangle c_\beta \langle b_\beta\rangle (S_{\alpha\beta}(Q)-1) \qquad\qquad 1.2.6$$

In neutron scattering the nucleus recoils under neutron impact and so the neutron can exchange energy with the scattering system (an "INELASTIC" collision). Hence even with diffraction experiments, dynamic effects almost invariable have to be considered. These are described by the van Hove dynamic structure factor, $S(Q,\omega)$. [3], with separate terms for self and interference scattering as before. The single atom term for atom α will be represented here by $S_\alpha(Q,\omega)$, and the interference term between α and β by $S_{\alpha,\beta}(Q,\omega)$. In terms of these quantities the so-called "STATIC STRUCTURE FACTORS" are defined by

$$S_\alpha(Q) = \int_{-\infty \text{ const. } Q}^{\infty} S_\alpha(Q,\omega)\, d\omega \qquad = 1$$

$$1.2.7$$

$$S_{\alpha\beta}(Q) - 1 = \int_{-\infty \text{ const. } Q}^{\infty} S_{\alpha\beta}(Q,\omega)\, d\omega \qquad = 1$$

Where the integrals are taken along a path of constant Q. It will be readily apparent that the diffraction experiment ideally should intergrate $S(Q,\omega)$ over all energy transfers and so obtain an ensemble from the ELASTIC diffraction experiment which probes on $S(Q,0)$ and so determines the residual structure after waiting a long time ($t=\infty$).

In terms of these partial dynamic structure factors the total dynamic structure factor for a material is defined in the same way as (1.2.3):

$$F(Q,\omega) = \Sigma\alpha\, c\alpha\, <b\alpha2>\, S\alpha(Q,\omega) + \Sigma_{\alpha,\beta}\, c_\alpha\, <b_\alpha>\, c_\beta\, <b_\beta>\, S_{\alpha\beta}(Q,\omega) \qquad 1.2.8$$

The inelasticity associated with the scattering causes a particular effect in that neutrons can arrive either earlier or later than they would have done if the scattering were elastic (no exchange of energy). If k and k' are the neutron wavevectors before and after the scattering, then the TIME-OF-FLIGHT-EQUATION states that

$$L / k + L' / k' = (L + L') / k_e$$

Where L is the incident flight path, moderator to sample, L' is the flight path from sample to detector and k_e is the elastic wavevector for a particular time channel. The TOF equation combines with the usual kinematic equations for the neutron:

$$Q^2 = k^2 + k'^2 - 2kk' \cos 2\theta \qquad\qquad 1.2.10$$

And

$$2m\hbar\omega = \hbar^2 k^2 - \hbar^2 k'^2 \qquad\qquad 1.2.11$$

to define the path through (Q,ω) space over which $F(Q,\omega)$ is integrated. Hence instead of measuring (1.2.3) for the time of flight directly, as we would ideally like to do, the TIME-OF-FLIGHT DIFFERENTIAL CROSS SECTIONS TDSC, is obtained in practice:

$$\Sigma(Q_e,\theta) = \int \frac{k'}{k} \, F(Q,\omega) \, \frac{\Phi(k)}{\Phi(k_e)} \left(\frac{\delta k}{\delta k_e}\right) \frac{E(k')}{E(k_e)} \, d\omega \qquad 1.2.12$$

Where $\Phi(k)$ is the incident spectrum expressed as a funtion of k, as described in section 1.1, $E(k')$ is the detector efficiency at the final wave vector, k_e is the wavevector for elastic scattering, and $Q_e=2k_e\sin\theta$. The dependence of Σ on θ is shown to emphasize that for a given value the TDCS is still a function of scattering angle. The partial derivative can be evaluated using 1.2.11 in 1.2.9:

$$(\delta k/\delta k_e)_\omega = (1+R)k^2/k_e^2 \, / \, 1+ Rk^3/k^3 \qquad 1.2.13$$

Where $R = L'/L$. Egelstaff [4] calls this a "sampling factor" because it controls the way $F(Q,\omega)$ is sampled.

Note that the TDCS is to be distinguished from the differential cross section (1.2.4) by virtue of the finite final flight path: if R were to go to zero then the TDCS is identical to the differential cross section. The denominators in equation (1.2.12) imply that the measured data have been normalized to the incident beam and detector efficiencies at the elastic scattering energy. This is achieved in practive by dividing the TOF data by the scattering from a standard sample, usually vanadium, which scatters almost entirely incoherently. Even so some spectrum dependence is found in the TDCS because of the inelastic scattering of some detected neutrons.

Strictly speaking the integral in (1.2.12) implies we cannot do the experiment because we don't know $F(Q,\omega)$, and even if we measured it we could never obtain it over a wide enough ω range to perform the integrals in (1.2.4) accurately. However, as has been shown by Placzek [5] and many others since then [e.g. 4, 6-13], the difference between $F(Q)$ and $\Sigma(Q,\theta)$ is small enough in many cases that we can estimate the difference

$$P(Q,\theta) = F(Q) - \Sigma(Q,\theta) \qquad 1.2.14$$

By using an approximate model for $F(Q,\omega)$. For example, such a model might satisfy the first two moments of the true $F(Q,\omega)$, which are often known. $P(Q,\theta)$ is called the PLACZEK or INELASTICITY CORRECTION, and note that it too is a function of both Q and θ.

There is a different Placzek correction for each term in (1.2.3), so we label the single atom Placzek correction as $P_\alpha(Q,\theta)$ and the interference correction as $P_{\alpha\beta}(Q,\theta)$. Each Placzek correction has to be evaluated by an integral like (1.2.12), but with $F(Q,\omega)$ replaced by the appropriate partial dynamic structure factor. There are several approximate ways of doing this, either by putting in a model for $S(Q,\omega)$, or else by a Taylor expansion about the static values. With the exception of simple molecules it is normally not possible to evaluate the interference Placzek correction, which however is expected to be small (see section 2.10 for further details).

With these definitions we can rewrite (1.2.12) in a form similar to (1.2.3):

$$F(Q) = \sum_\alpha c_\alpha <b_\alpha^2> [1 + P_\alpha(Q,\theta)] + \sum_{\alpha,\beta} c_\alpha <b_\alpha> c_\beta <b_\beta> [S_{\alpha\beta}(Q) -1 + P_{\alpha,\beta}(Q,\omega)]$$

$$1.2.15$$

The basic steps in the data analysis should now be apparent:

(1) Derive $\Sigma(Q,\theta)$ from a set of diffraction data;
(2) Estimate and subtract the single atom scattering, i.e. the first term in (1.2.15);
(3) Derive g(r) after removing any interference Placzek corrections.

The bulk of this manual is concerned with the first of these steps, although we will also suggest ways of tackling the other two stages.

SECTION 2:

STEPS IN DATANALYSIS OF TOF DIFFRACTION DATA: THEORY

2.1 The analysis of TOF diffraction data

The initial goal of the experimenter is to obtain the TDSC of his or her sample. The success of subsequent analysis to g(r) or partial structure factors depends critically on obtaining the TDCS accurately. A number of corrections are required to the measured data. The corrections are straightforward to apply but non the less easy to get wrong. Four main sources of error can be identified:

(i)   The experimenter doesn't have complete information about his or her sample, e.g. dimensions, densities, cross sections, etc.
(ii)   Incorrect data analysis procedures are used.
(iii)   The detectors are not sufficiently stable.
(iv)   Sample environment equipment introduces unexpected backgrounds and sample positioning errors.

The last two causes require action by the instrument scientists, but there is little or nothing that can correct for poorly characterised samples or incorrect data analysis procedures.

With the exceptions of sections 2.9 and 2.11, which concern the estimation of inelasticity corrections and transforming the final result to g(r), we believe the methods of analysis of diffraction data from liquids and amorphous samples are well understood and routine. In the sections which follow, we have attempted to describe the correct sequence of steps.

As seen in section 1.1, the scattered intensity is measured as a function of time-of-flight which in turn is proportional to wavelength. The data can also be presented as a function of wave vector, k, wave vector transfer, Q, or energy, E, by using the relationships (1.1.5) to apply the appropriate rescaling. The choice is subject to the preference of the experimenter, although the Q representation is the most common as it relates to the reciprocal space in which the structure factor is defined, equation (1.2.1). Therefore, we shall use the Q representation here. If a sample is very small so that it is possible to neglect the effects of attenuation and multiple scattering, the detected count rate would be proportional to the incident flux, $\Phi(k_e)$. The TDCS of the sample, $\Sigma(Q_e)$, the detectir solid angle, $\Delta\Omega$, and the detector efficiency $E_d(k_e)$:

$$I(k_e) = \Phi(k_e)\, N\, \Sigma(Q_e)\, E_d(k_e)\, \Delta\Omega \qquad\qquad 2.1.1.$$

Where N is the number of scattering units in the neutron beam, and $Q_e = 2k_e \sin\theta$. The incident flux and the detector efficiency are represented here as a function of k_e to emphasize that they are not a function of the scattering angle of the detector.

Equation (2.1.1) is an idealized count rate: the first correction that must be applied is for detector deadtime.

2.2 Deadtime corrections

No matter how well made, a detector is always "dead" for a short period of time after a neutron event has occurred. For a ^{3}He tube this DEADTIME might be 3μs, whilst for a glass scintillator it is perhaps 250ns, before another event can be recorded. The zinc sulphide detectors will have a deadtime between 2 and 10μs, depending on how they are setup. Normally the correction for deadtime is a few percent and so can be made by a simple formula. Suppose τ is the deadtime in μs for a detector. First consider the case where the time

channel is broad compared to the deadtime. If R_m is the measured count rate in the time channel (in cts/μs), then the detector is dead for a time:

$$D = \Delta R_m \tau \qquad\qquad 2.2.1$$

Where Δ is the width of the time channel in μs. Hence the count rate, R, which would have been measured if the detector had zero deadtime, is greater than R_m in proportion to the time that the detector is dead:

$$R = [\Delta/(\Delta-D)]\, R_m = R_m\,/\,(1 - R_m\tau) \qquad\qquad 2.2.2$$

At the other extreme, if the time channels are narrower than the deadtime, then some of the previous time channels may contribute to the deadtime in a particular channel. For example, if channels n to m contribute to the deadtime in channel M, then the length of time channel m is dead is given by:

$$D_m = \tau \sum_{j=n,m} \Delta_j R_j \qquad\qquad 2.2.3$$

Where Δ_j and R_j are the channel width and count rate in channel j respectively. The limits of j are determined by inspection. This correction is used in the same way as before, with D_m in place of D in (2.2.2).

A subtlety occurs in practice that renders the correction more complex. When many detectors exist it is not practical to have a separate input for each detector into the DAE. Instead an ENCODER is used to create a binary address which describes which detector is fired. If the deadtime of the encoder is longer than that of the detector, then it is the encoder's deadtime which determines the detector deadtime. Moreover since the encoder can process only one event at a time, **all** the detectors that feed into that encoder are effectively dead when any one detector fires. Therefore in this situation the sum in (2.2.3) should include a sum over all channels which feed into a decoder. In that case the $R_{j,k}$ is the count rate in time channel j and encode channel k, then the detector deadtime is given by:

$$D_m = \tau \sum_{j=n,m} \sum_k \Delta_j R_{j,k} \qquad\qquad 2.2.4$$

And the sum over k is over all detector channels that feed into the encoder. In the situation when (2.2.4) applies Δ_j is the encoder's deadtime, NOT the detector's. Hence even though the deadtime for an individual detector may be small, the grouping of say 50 detectors into an encoder can result in a 50-fold enhancement in the count rate as far as deadtime is concerned. So the deadtime correction could be much larger than might be apparent from the count rate in an individual detector.

Note: with the current analysis procedures for SANDALS data, this correction is found to be largely unnecessary.

2.3 Normalisation to the incident beam monitor

Having corrected $I(Q_e)$ for deadtime, the next stage is to divide out the incident spectrum, which is measured by means of a MONITOR detector placed in the incident beam before the sample. The spectrum is divided out at this stage because small variations in moderator

temperature and proton beam steering can modify the energy dependence of the spectrum from time to time at the 1-2% level. Since the calibration run must be performed before or after the sample run, it will only give a reliable result if the dependence on the incident spectrum is removed at the end of each run. The count rate in the monitor detector, which of course must also be corrected for deadtime, is proportional only to the incident spectrum and the monitor efficienct:

$$I_m(k_e) = \Phi(k_e) \, E_d(k_e) \qquad\qquad 2.3.1$$

Thus when used to normalise the scattered neutron count rate, a NORMALISED count rate is obtained:

$$NRM(k_e) = I(k_e)/I_m(k_e) = N \, \Sigma(Q_e) \, [E_d(k_e)/E_m(k_e)] \, \Delta\Omega \qquad\qquad 2.3.2$$

A second measurement which is made at the same time as the scattered count rate from the sample is the fraction of neutrons transmitted by the sample. This number is monitored by a TRANSMISSION MONITOR, with efficiency $E_t(k_e)$, placed after the sample. Again this fraction cannot be measured directly, but must be determined by ratioing different runs, e.g. with and without sample. If $I_t(k_e)$ is the count rate in the transmission monitor, then this count rate is proportional to the incident flux, the transmission monitor efficiency and the TRANSMISSION of the sample, $T(k_e)$, which will be defined in the next section and is dependent on the total neutron cross section of the sample. Hence, when normalised to the incident monitor, the transmitted intensity is given by:

$$MON(k_e) = I_t(k_e)/I_m(k_e) = T(k_e) \, [E_t(k_e)/E_m(k_e)] \qquad\qquad 2.3.3$$

The transmission monitor is used to provide information on the neutron cross section and density of the sample: it can often confirm that the sample is what it is supposed to be.

There will then be a set of NRM (or SUM) files for every detector or detector group, and a MON file for every run, whether it be sample, container, vanadium (calibration) or background. The stages covered by sections 2.2 and 2.3 are obtained by running the NORM program.

2.4 Measuring the neutron cross section

(a) The total neutron cross section

Neutron cross sections arise from two primary processes: scattering and capture. Provided there are no nuclear resonances in the energy region of interest, the probability for capture is inversely proportional to the neutron velocity, i.e. proportional to neutron wavelength, and the constant of proportionality, usually defined for $2200 \mathrm{ms}^{-1}$ neutrons ($\lambda=1.8\text{Å}$), is called the CAPTURE CROSS SECTION, σ_a. There is a value of σ_a for every nucleus although in many cases it is quite small or zero.

The SCATTERING CROSS SECTION, $\sigma_s(\lambda)$, on the other hand has no such simple dependence on energy or wavelength, because it represents the integral of the DIFFERENTIAL SCATTERING CROSS SECTION, $d\sigma/d\Omega$ at a particular wavelength over all scattering angles:

$$\sigma_s (\lambda) = \int \frac{d\sigma}{d\Omega} (\lambda)\, d\Omega \ = \ 4\pi \int \frac{d\sigma}{d\Omega} (\lambda)\, \sin 2\theta\, d\theta \qquad\qquad 2.4.1$$

As an example of the application of this result we will assume the static approximation applies and that the liquid under investigation is a hard sphere fluid of reduced density $\rho\sigma^3 =$ 0.5, where σ, the hard core diameter, is 3.142Å. In that case S(Q) is known exactly in the Percus-Yevick approximation, and so (2.4.1) can be integrated numerically for all wavelengths using:

$$\frac{d\sigma}{d\Omega} (\lambda) = b^2 S(Q) = b^2 S(4\pi \sin\theta/\lambda) \qquad\qquad 2.4.2$$

where b is the bound scattering length of the fictitious nucleus. The result is shown in figure 2.1.

TITLE : Total hard sphere cross section
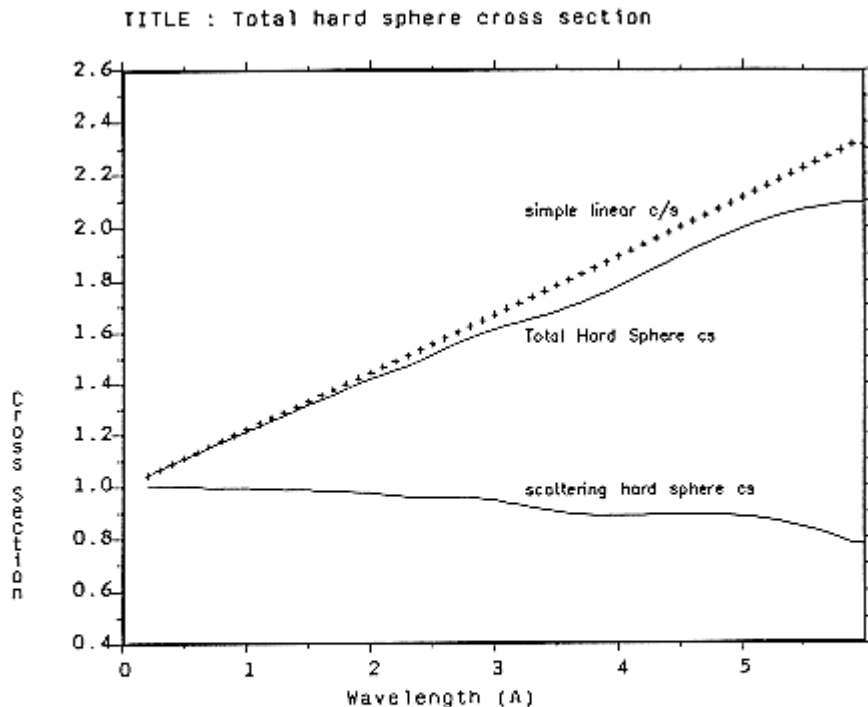
Figure 2.1 Calculated scattering and total cross section for a hard sphere fluid of density $\rho\sigma^3 = 0.5$, with $\sigma=3.142$. The fluid is assumed to have unit scattering cross section per atom, and the capture cross section is 0.4 at 1.8Å. The crosses correspond to a structureless fluid

It will be seen that the scattering cross section for a material with structure will certainly deviate from the bound value. In particular the scattering cross section will display a similar structure to that seen in the differential scattering cross section.

For light atoms such as hydrogen and deuterium the consequences are quite drastic: the differential cross section falls dramatically with scattering angle at all but the longest neutron

wavelengths, and the shape of the fall, which depends on the details of $S(Q,\omega)$, also varies with energy. Thus at low energies the neutron can excite only diffusional type motions, while at high energies the neutron can excite all possible modes, including dissociation of molecules if present. Thus the scattering cross section must vary between its so-called "BOUND" and "FREE" values as we go from low energy to high. The "bound" values are those quoted in tables of neutron scattering lengths such as the compilation by Koester et. Al. [14] or Sears [15] and correspond to the case of an immovable nucleus: they are essentially nuclear parameters. The corresponding "free" values at high energies can be computed by multiplying the "bound" cross sections by the ratio

$$[A/(A+1)]^2$$

where A is the mass of the nucleus in question. This has the value 0.25 for hydrogen and 0.44 for deuterium, which tells us to expect a large fall in the scattering cross section of these materials with increasing energy. Such a fall is readily visible in the transmission data from hydrogen containing samples. For heavy atoms on the other hand this factor is close to unity and so within the likely accuracy of the transmission measurement, is not significant.

In practice it also shows a second quantity, the TOTAL NEUTRON CROSS SECTION, $\sigma_t(\lambda)$, where:

$$\sigma_t(\lambda) = \sigma_s(\lambda) + \sigma_a(\lambda) \qquad\qquad 2.4.3$$

In this case it has been assumed that the fictitious material has a capture cross section $\sigma_a = 0.4$ at $\lambda = 1.8\text{Å}$. It can be seen that the approximation of treating the total cross section as a sum of a constant plus linear term in λ will be inadequate for accurate work at long wavelengths.

If nuclear resonances are present in the total cross section, then the above treatment must be modified. A nuclear resonance occurs when the neutron excites the nucleus to an excited state, and so is (slightly) analogous to an absorption edge in X-ray scattering. However, the possible nuclear states are quite complicated in general and can be accompanied by several processes, including the emission of a γ photon. Usually both scattering and capture are not simple at a resonance, and full treatment of the effects of this on the data analysis are beyond the present purpose, and certainly are not included in any of the correction routines. At present the only recourse is to ignore the energy regions where resonances occur and hope that there is sufficient angular coverage that all Q values can be obtained away from a resonance. Figure 2.2 shows the measured cross section for a solution of [148]Sm-perchlorate in D_2O. Note the strong resonance at $\lambda \approx 1$ Å, corresponding to a nuclear resonance in a [149]Sm impurity. This resonance was so broad that analysis of these data to TDCS was impossible. Appendix E lists the more commonly occurring resonances.

TITLE : Sm148 perchlorate in D2O
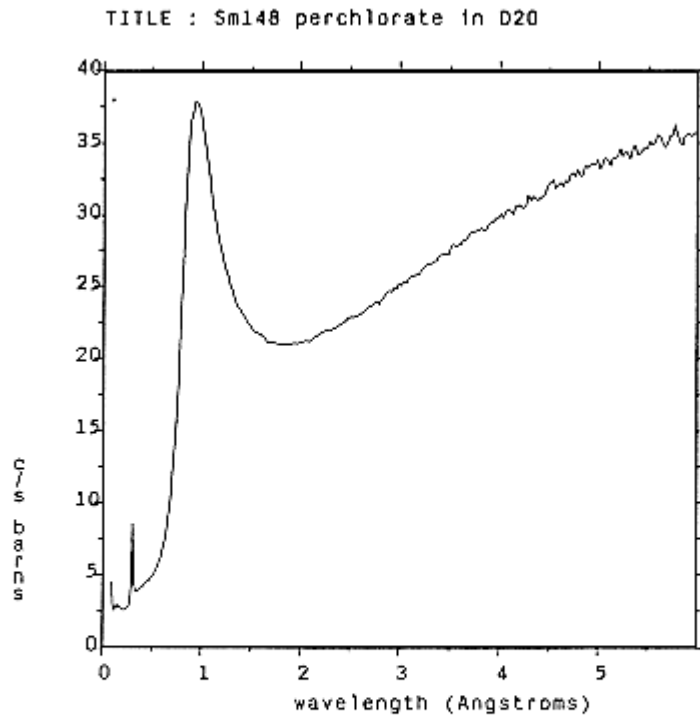
Figure 2.2   Measured transmission cross section for a solution of ^{148}Sm-perchlorate in D$_2$O. Note the pronounced neutron resonance near $\lambda=1\text{Å}$ which arises from a ^{149}Sm impurity. Higher energy resonances are visible at shorter wavelengths.

(b) Measuring the neutron cross section

We have seen above that the total cross section depends on the STRUCTURE and DYNAMICS of the sample, which in turn relates to the thermodynamic state of the sample. Therefore it strictly has to be measured for each and every sample, and this is why a transmission monitor is placed after the sample. In practice it is difficult to measure the total cross section on an ABSOLUTE scale with the necessary precision, so the transmission monitor is used to obtain the ENERGY DEPENDECNE of the total cross section, with absolute values obtained by reference to the known free and bound values at short and long wavelengths. Note that using a separate experiment to measure transmissions is very time consuming and not necessarily useful since it is not always possible to reproduce the exact conditions of the experiment at a later time.

If the sample is a flat plate which uniformly covers the beam, then the TRANSMISSION of the sample is given simply by:

$$T(k_e) = \exp \{-\rho\sigma_t(\lambda)L\} \qquad\qquad 2.4.4$$

Where ρ is the number density and L is the neutron flight path within the sample. Hence if $T(k_e)$ can be obtained from monitor ratios as described in section 2.3 then it is a trivial inversion to obtain σ_t.
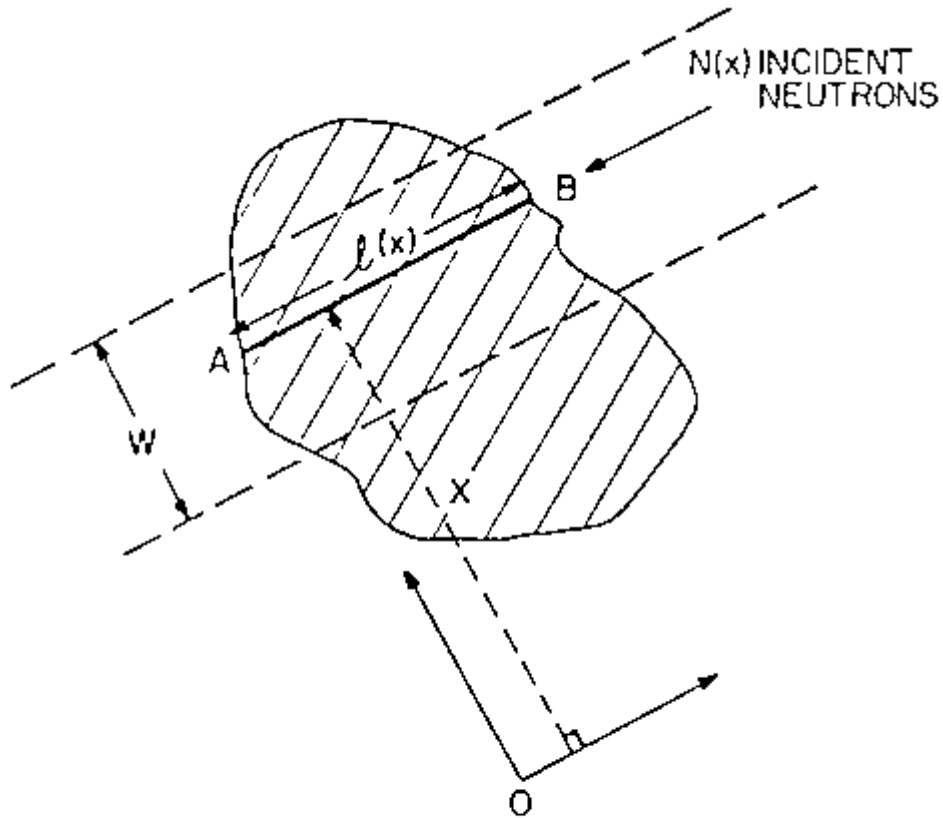
Figure 2.3 Geometry of transmission problem for an arbitrary shaped sample

For any other shape of sample however, the flight path through the sample is a function of position within the beam. Figure 2.3 shows the geometry of the problem in this case. If x measures the perpendicular distance from one edge of the beam the L becomes a function of x and the transmission in this case can be written as:

$$T(k_e) = \int_0^W \exp\{-\rho\sigma_t(\lambda)L(x)\}\, dx\, /\, W \qquad\qquad 2.4.5$$

where W is the width of the beam. In this case there is no simple inversion to σ_t, which has to be obtained by trial and error. However if a Newton-Raphson technique is used to do this, convergence to a solution is quite rapid. Further efficienct can be gained by noting that only a finite number of terms in the exponential are needed. Writing $\mu = \rho\sigma_t$, we see that

$$T(k_e) = 1 - \mu M_1 + (\mu M_2)^2 - (\mu M_3)^3 + \dots \qquad\qquad 2.4.6$$

Where

$$M_n = (1/n!) \int_0^W L^n(x)\, dx\, /\, W \qquad\qquad 2.4.7$$

The latter integrals are dependent only on the shape of the sample and not on neutron energy and so need only be evaluated once.

If the sample is contained in a holder then the monitor ratio that is used, is the ratio of sample plus can, to can alone. In that case the measured transmission is given by

$$T(k_e) = \frac{\int_0^W \exp\{-[\mu_s L_s(x) + \mu_c L_c(x)]\}\,dx}{\int_0^W \exp\{-\mu_c L_c(x)\}\,dx} \qquad\qquad 2.4.8$$

where the suffix S applies to the sample and C applies to the container. Similar expansions of the top exponential term can be used as before. However the values of μ_c must be supplied separately or obtained in a separate transmission experiment on the container alone. Finally note that if the beam profile is not uniform, a simple modification to the above formulae is needed: because the profile function can be included in the moments (2.4.7) it does not lead to any increase in computing time.

2.5 Attenuation and multiple scattering corrections

Much of the underlying methodology for calculating ATTENUATION and MULTIPLE SCATTERING corrections has been covered in numerous previous publications and so will not be repeated here. Although there are a number of approaches to the calculation, the formalism of Soper and Egelstaff [16], which uses numerical integrations to estimate corrections for the cylindrical geometry, is used here, because it is written in a sufficiently general form to allow corrections for furnaces and radiation shields if they are sufficiently absorbing or scattering to require a separate correction. These latter corections will be the subject of the next section.

The most common case is that of a sample contained in a holder. In that case two measurements are needed: one for the sample plus can, $I_{SC}(k_e)$, and one for the can alone $I_C(k_e)$. These two quantities are each affected by attenuation and multiple scattering so our simple definition (2.1.1) has to be modified for the general case:

$$I_{SC}(k_e) = \Phi(k_e)[N_S\Sigma_S(Q_e)A_{S,SC} + N_C\Sigma_C(Q_e)A_{C,SC} + M_{SC}(k_e)]\,E_d(k_e)\Delta\Omega \qquad 2.5.1$$

$$I_C(k_e) = \Phi(k_e)[N_C\Sigma_C(Q_e)A_{C,C} + M_C(k_e)]\,E_d(k_e)\Delta\Omega \qquad\qquad 2.5.2$$

Here N_S and N_C are the number densities of atoms in the sample and container respectively, while $A_{S,SC}$, $A_{C,SC}$, and $A_{C,C}$ are the usual Paalman and Pings [17] attenuation factors. For example, $A_{S,SC}$ is the attenuation factor for scattering in the sample and attenuation in the sample plus container. The quantities M_{SC} and M_C are the total multiple scattering differential scattering cross sections for sample plus can and can alone respectively. Note that the multiple scattering terms cannot in general be included in first scattering terms because the are not linear in N_S and N_C. Both attenuation and multiple scattering terms are functions of neutron energy by nirtue of the energy dependence of the scattering and capture cross sections.

The attenuation factors depend only on the sample geometry and the total neutron cross section and so can be evaluated exactly in the static approximation, within the limits of numerical precision.

On the other hand, the multiple scattering terms can never be evaluated very accurately since in principle they require detailed knowledge of the sample's structure (and dynamics if the inelastic scattering is significant). The method of calculation normally employed makes use of the measured total transmission cross section to give the scattering cross section at each neutron energy, but then assumes the scattering at this energy to be isotropic with scattering angle. This is called the ISOTROPIC approximation. (This is NOT the same as assuming that the multiple scattering is isotropic, an approximation introduced by Blech and Averbach [18] which is not needed in practive.) Sears [19] has described how the isotropic approximation can be improved although direct calculation with a Monte Carlo algorithm which includes the measured TDCS is probably the best way to cope with multiple scattering from thick samples. Given the speed of modern computers this is not an unreasonable approach. Howells has a program, ELMS, (Elastic Multiple Scattering) which does this and it can be made available if there is sufficient demand.

There is a general consensus that the isotropic approximation is expected to be acceptable if the sample scatters less than ~20% of the incident beam, although there has never been a quantitative study of the size of sample at which this approximation starts to introduce a serious systematic error in the measured structure factor. Clearly it greatly assists the multiple scattering problem if the container can be made of an incoherent scatterer, such as vanadium or titanium-zirconium, or of an amorphous material such as silica, since Bragg peaks introduce severe difficulty to any quantitative multiple scattering calculation.

In summary, to be confident that multiple scattering will not introduce too large a systematic error it is a useful rule of thumb to ensure that the sample scatters between 10% and 20% of the incident neutron beam.

2.6 Furnace corrections

If the sample and container are in a furnace and the furnace element contributes significantly to the attenuation and scattering processes, then three measurements are needed: sample + can + furnace, $I_{SCF}(k_e)$, empty can + furnace, $I_{CF}(k_e)$, and furnace alone, $I_F(k_e)$. These three quantities are related to the corresponding differential cross sections by:

$$I_{SCF}(k_e)= \Phi(k_e)[N_S\Sigma_S(Q_e)A_{S,SCF} + N_C\Sigma_C(Q_e)A_{C,SCF} + N_F\Sigma_F(Q_e)A_{F,SCF} + M_{SCF}(k_e)]$$
$$\times E_d(k_e)\Delta\Omega$$

$$2.6.1$$

$$I_{CF}(k_e) = \Phi(k_e)[N_C\Sigma_C(Q_e)A_{C,CF} + N_F\Sigma_F(Q_e)A_{F,CF} + M_{CF}(k_e)] E_d(k_e)\Delta\Omega \qquad 2.6.2$$

$$I_F(k_e) = \Phi(k_e)[N_F\Sigma_F(Q_e)A_{F,F} + M_F(k_e)] E_d(k_e)\Delta\Omega \qquad 2.6.3$$

The attenuation factors have the same definition as before, e.g. $A_{S,SCF}$ is the attenuation factor for scattering in the sample and attenuation in the sample, can and furnace. Similarly the multiple scattering cross sections have an equivalent definition as before. N_F is the number of furnace atoms in the incident beam.

2.7 Vanadium or standard sample calibration

A unique characteristic of neutron scattering is the ability to perform an independent estimate of the instrumental calibration. This calibration consists of the unknown quantities, either

$$F_1(k_e) = \Phi(k_e)\, E_d(k_e)\Delta\Omega \qquad\qquad 2.7.1$$

In sections 2.1, 2.5 and 2.6 above or

$$F_2(k_e) = [E_d(k_e)/E_m(k_e)]\, \Delta\Omega \qquad\qquad 2.7.2$$

In section 2.3. with these definitions we can for example rewrite equations (2.5.1) and (2.5.2) which become, after normalizing to the monitor:

$$NRM_{SC}(Q_e) = F_2(k_e)[N_S\Sigma_S(Q_e)A_{S,SC} + N_C\Sigma_C(Q_e)A_{C,SC} + M_{SC}(k_e)] \quad 2.7.3$$

$$NRM_C(Q_e) = F_2(k_e)[N_C\Sigma_C(Q_e)A_{C,C} + M_C(k_e)] \qquad\qquad 2.7.4$$

Estimation of these calibration constants is usually achieved with a standard vanadium sample because vanadium has a largely incoherent cross section and so it is believed that the differential cross section for vanadium can be estimated reasonably accurately, an assumption which of course is difficult to check! As described in section 2.9 the inelasticity correction has two principal terms, one relating to scattering angle, the other proportional to temperature and inversely proportional to neutron energy, and since energy is being varied is a TOF experiment it is crucial to estimate this latter term correctly. Figure 2.4 shows the estimated single atom differential cross section at 20º scattering angle for a free vanadium nucleus at two temperatures.

The normalised spectrum from vanadium is defined by

$$NRM_V(Q_e) = F_2(k_e)[N_V\Sigma_V(Q_e)A_{V,v} + M_V(k_e)] \qquad\qquad 2.7.5$$

The quantity in square brackets is the vanadium differential cross section which is estimated using exactly the same methods as in the previous section. This leads to a VANADIUM CALIBRATION, $CAL_V(Q_e)$, where

$$CAL_V(Q_e) = NRM_V(Q_e)\, /\, [N_V\Sigma_V(Q_e)A_{V,v} + M_V(k_e)] = F_2(k_e) \qquad 2.7.6$$

In fact, scattering from vanadium exhibits the usual statistical noise plus weak Bragg reflections due to the small coherent scattering amplitude. Since the data from the sample must be divided by CAL_V it is obviously undesirable to transfer either effect to the sample data, so an expansion in terms of Chebyshev polynomials is fitted to NRM_V with zero weighting of points in the region of Bragg peaks. This has the effect of smoothing out the Bragg peaks and noise without introducing any appreciable artifacts. However, it is clearly important to check that this smoothing has in fact removed only the noise from NRM_V and none of the underlying structure. In any case whether to smooth or not is an option which can be overridden if needed.

TITLE : Placzek correction for vanadium at 20 deg.
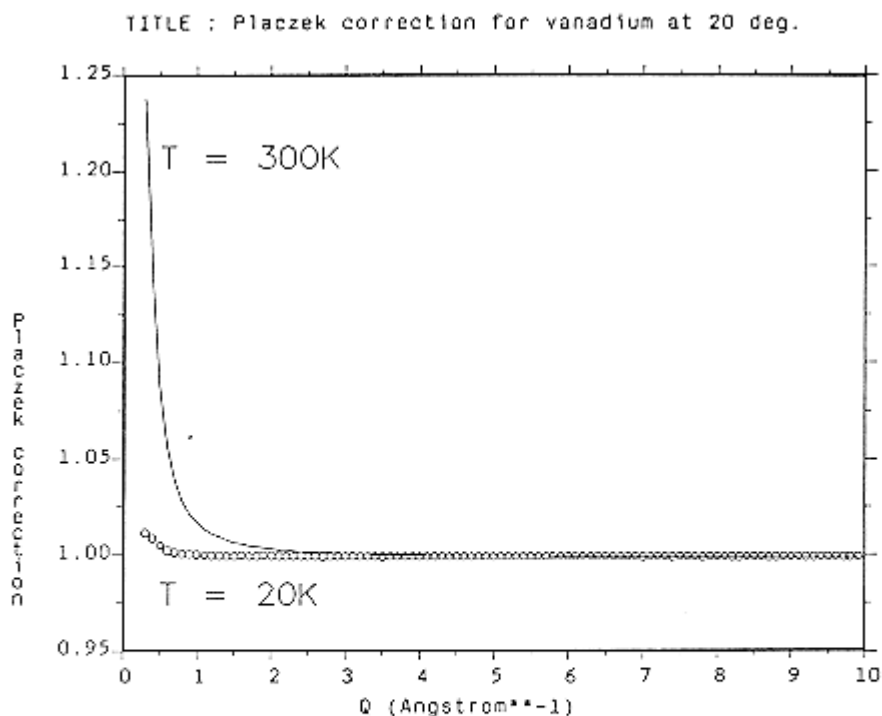
Figure 2.4 Calculated TOF recoil correction (1+P) for a free vanadium nucleus at two temperatures: 20K and 300K, and at a scattering angle of 20°. Note the large temperature effect at small Q values.

2.8 Basic algorithm to determine the differential cross section

All of the main quantities needed to calculate the differential cross section (DCS) from the TOF diffraction data have now been described, and the algorithm ANALYSE is used to perform this operation. The stages are described in sequence for the case of a sample held in a can. Note that the arrow $\Rightarrow$ is used to indicate that the result of an operation on the left hand side is placed in the quantity on the right. The symbol TOTAL applies to the total scattering, SINGLE applied to the single scattering, and the suffixes S,C and B refer to the sample, can and background.

(1) Subtract background

$$\text{TOTAL}_{SC}(Q_e) = \text{NRM}_{SC}(Q_e) - \text{NRM}_B(Q_e)$$

$$\text{TOTAL}_C(Q_e) = \text{NRM}_C(Q_e) - \text{NRM}_B(Q_e)$$

(2) Normalize to calibration

$$\text{TOTAL}_{SC}(Q_e) \Rightarrow \text{TOTAL}_{SC}(Q_e) / \text{CAL}_V(Q_e)$$

$$\text{TOTAL}_C(Q_e) \Rightarrow \text{TOTAL}_C(Q_e) / \text{CAL}_V(Q_e)$$

28

(3) Subtract multiple scattering

$$SINGLE_{SC}(Q_e) = TOTAL_{SC}(Q_e) - M_{SC}(k_e)$$

$$SINGLE_C(Q_e) = TOTAL_C(Q_e) - M_C(k_e)$$

(4) Apply absorption corrections

$$SINGLE_S(Q_e) = (SINGLE_{SC}(Q_e) - SINGLE_C(Q_e) [A_{C,SC}/A_{C,C}]) / A_{S,SC}$$

(5) Divide by number of atoms in sample

$$DCS(Q_e) = SINGLE_S(Q_e) / N_S$$

If the furnace correction is being applied then the following modified sequence is used:-

(1) Subtract background

$$TOTAL_{SCF}(Q_e) = NRM_{SCF}(Q_e) - NRM_B(Q_e)$$

$$TOTAL_{CF}(Q_e) = NRM_{CF}(Q_e) - NRM_B(Q_e)$$

$$TOTAL_F(Q_e) = NRM_F(Q_e) - NRM_B(Q_e)$$

(2) Normalize to calibration

$$TOTAL_{SCF}(Q_e) \Rightarrow TOTAL_{SCF}(Q_e) / CAL_V(Q_e)$$

$$TOTAL_{CF}(Q_e) \Rightarrow TOTAL_{CF}(Q_e) / CAL_V(Q_e)$$

$$TOTAL_F(Q_e) \Rightarrow TOTAL_F(Q_e) / CAL_V(Q_e)$$

(3) Subtract multiple scattering

$$SINGLE_{SCF}(Q_e) = TOTAL_{SCF}(Q_e) - M_{SCF}(k_e)$$

$$SINGLE_{CF}(Q_e) = TOTAL_{CF}(Q_e) - M_{CF}(k_e)$$

$$SINGLE_F(Q_e) = TOTAL_F(Q_e) - M_F(k_e)$$

(4) Subtract furnace from sample and can

$$SINGLE_{SC}(Q_e) = (SINGLE_{SCF}(Q_e) - SINGLE_F(Q_e)[A_{F,SCF} / A_{F,F}])$$

$$SINGLE_C(Q_e) = (SINGLE_{CF}(Q_e) - SINGLE_F(Q_e)[A_{F,CF} / A_{F,F}])$$

(5) Apply absorption corrections

$$SINGLE_S(Q_e) = (SINGLE_{SC}(Q_e) - SINGLE_C(Q_e) [A_{C,SCF} / A_{C,CF}]) / A_{S,SCF}$$

(6) <u>Divide by number of atoms in sample</u>

$$DCS(Q_e) = SINGLE_S(Q_e) / N_S$$

2.9 Inelasticity (Placzek) corrections

Equations 1.2.9, 1.2.11 and 1.2.12 serve to define the inelasticity correction, $P(Q_e,\theta)$ in a TOF diffraction experiment: $P(Q_e, \theta)$ represents the difference beetween the static approximation $F(Q)$ and the TDCS, $\Sigma(Q_e)$. Strictly speaking to obtain $P(Q_e,\theta)$, one needs to know $F(Q,\omega)$ which preempts the need for a diffraction experiment since then the static structure factors (1.3.4) would be obtainable by direct integration of $F(Q,\omega)$. Obviously this is an impractical proposition, mostly because of the time that would be required in measuring the complete dynamic structure factor.

However, in 1952 Placzek [5] showed that for nuclei much more massive than the neutron, the correction adopts a form which is essentially independent of the detailed dynamics, and is related only to the nuclear mass, the sample temperature, the incident neutron energy, and the geometry and efficiency of the neutron detection process. Moreover at neutron energies well above those of any bound states that occur in the sample, he showed that the correction to the interference term $S_{\alpha\beta}(Q)$ is zero to first order. These conclusions arose from the fact that the first two moments of $S(Q,\omega)$ can be estimated more or less exactly:

$$^1S_\alpha(Q) = \int_{-\infty}^{\infty} \omega S_\alpha(Q,\omega)d\omega = \frac{\hbar Q^2}{2M_\alpha} \qquad 2.9.1$$

$$^2S_\alpha(Q) = \int_{-\infty}^{\infty} \omega^2 S_\alpha(Q,\omega)d\omega = \frac{k_B T\hbar Q^2}{M_\alpha} + \frac{\hbar^2 Q^4}{4M_\alpha^2} \qquad 2.9.2$$

and

$$^1S_{\alpha\beta}(Q) = \int_{-\infty}^{\infty} \omega S_{\alpha\beta}(Q,\omega)d\omega = 0 \qquad 2.9.3$$

Here (2.9.1) and (2.9.3) are exact results, but (2.9.2.) strictly only applies to a classical fluid.

Unfortunately Placzek's results cannot always be applied directly to thermal neutron diffraction because the conditions under which they apply are often not obtained. In particular the sampling factor (equation 1.2.10) rapidly drops to zero as k; becomes less than k. Hence as in the fixed wavelength reactor experiment the scope fore exciting high vibrational levels in a molecule depends on the incident energy. There is an extensive literature on the attempts to modify the original Placzek approach to include the cases where the system is only partly excited by the neutron. See for example the papers by Powles [6-11] and Egelstaff [4,12,13]

and references therein. All of these involve lengthy algebra and while there seems to be general agreement in the case of the self scattering for an atomic fluid the correct form of the terms for molecules, which involve a Q-dependent effective mass is still displuted, The advantage of the Placzek type of expansion is that it enables one to understand by inspection the effect of various instrument parameters on the inelasticity correction. In particular on can examine the effect of the flight path ration, sample temperature, detector efficiency and incident spectrum shape.

As an example, below is quoted the Egelstaff [4] formula for the self scattering inelasticity correction for an atomic fluid of nuclear mass M at temperature T, for a 1/E incident spectrum, at incident energy E_0:

$$P(Q_e, \theta) = - (2ym/M) X + (m/M)[k_B T/2E_0] Y \qquad\qquad 2.9.4$$

Where

$$X = (aA + a + 2) / (a + 1)$$

$$Y = [1 - 2y + \{4y(Aa + 3)/(a+1)\} - \{2y[a^2 B - 6a(A+1) - 3(5a-1)] / (a+1)^2\}]$$

And $y = \sin^2\theta$, m = mass of neutron, a = 1/R = L/L', and A and B are detector constants:

$$A = 1 - (\varepsilon/k_e)[(1/E_{d(k_e)}) - 1]$$

$$B = A + (\varepsilon/k_e)^2[(1/E_{d(k_e)}) - 1]$$

With

$$E_{d(k_e)} = 1 - \exp(-\varepsilon/k_e)$$

And ε is a detector constant which determines the efficiency. Further terms are needed in the Maxwellian region.

This formula gives the quantitative behaviour of the Placzek correction at large neutron energies, but also indicates qualitatively what will happen at all energies. In particular we see that the correction gets notably larger at low neutron energies, high temperatures and at small nuclear masses. Hence the often quoted maxim that the ideal diffraction experiment is performed at high energies and small scattering angles. The routine PLATOM uses a modification of the Powles [10] formula derived by Howe, McGreevy and Howells [20]. Detailed comparison of this formula with the numerical methods described below shows some quantitative discrepancies which are not understood at the present time.

An alternative to the Placzek expansion is to define a model neutron scattering law $S(Q,\omega)$ which incorporates the properties defined in (2.9.1) and (2.9.2), or any alternative scattering laws which are known to represent $S(Q,\omega)$ correctly in the region of (Q,ω) space explored by experiment, and then performs the integral (1.2.9) numerically. This method is most useful when a particular scattering law is known to apply e.g. such as that for a diffusing particle or for a rigid molecular rotor, or when the neutron mass is small. In all these examples, the Placzek expansion is not helpful. Figure 2.5 shows a comparison between the numerical

integration of the free particle $S(Q,\omega)$ (ideal gas formula) and equation (2.9.4) for a nucleus of mass 51 (vanadium) and scattering angle of 20°. Note that at this small angle the expansion formula gives good agreement with the numerical calculation, but at larger angles such as 90° and 150° the agreement is much worse, although in every case the high Q limit is the same. Figure 2.6 shows the numerical calculation for a mass 2 particle at two temperatures. A pronounced temperature effect is seen. Moreover the correction now has a clear hump at ~2Å^{-1} corresponding to the derivative of the incident spectrum. Results such as this can only be obtained by numerical integration.

TITLE : Vanadium Placzek correction at 20 deg.
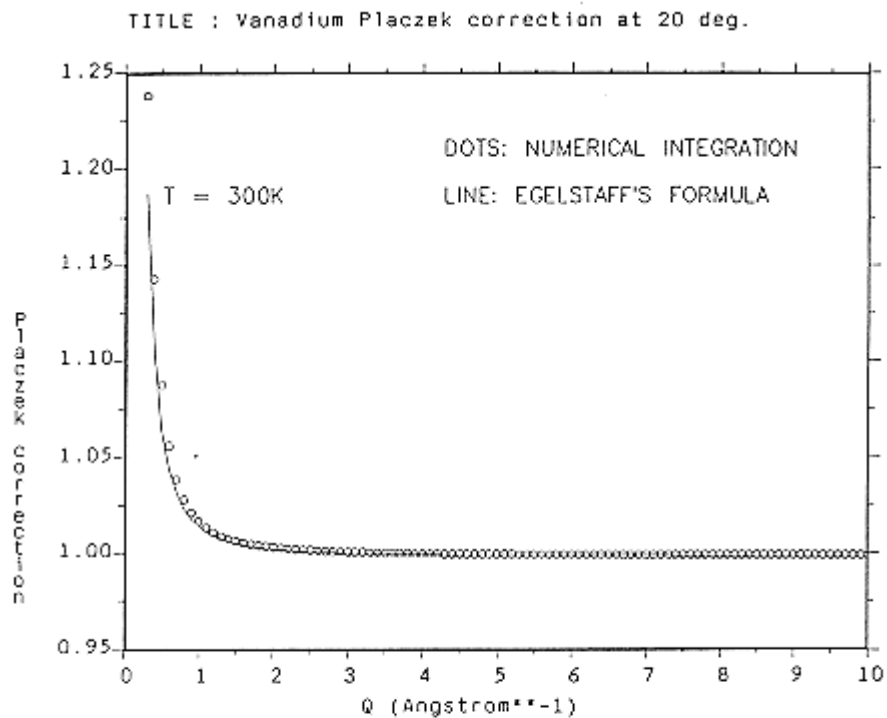
Figure 2.5 Comparison of numerical calculation of recoil correction for a vanadium nucleus at T=300K and scattering angle 20°, with Egelstaff's approximate formula, equation (2.9.4), which does not have the correct spectral dependence at small Q. Even so it gives good agreement at all Q values

Two computer programs exist to perform these numerical integrations: PLACID calculates the Placzek correction for an ideal gas, i.e. treating the particle as free. The other program is called PLATOF and it allows the user to input a table of $S(Q,\omega)$ values from a separate calculation. Both programs can be made available for general use if there is sufficient demand.

TITLE : Placzek correction for deuterium at 20 deg.
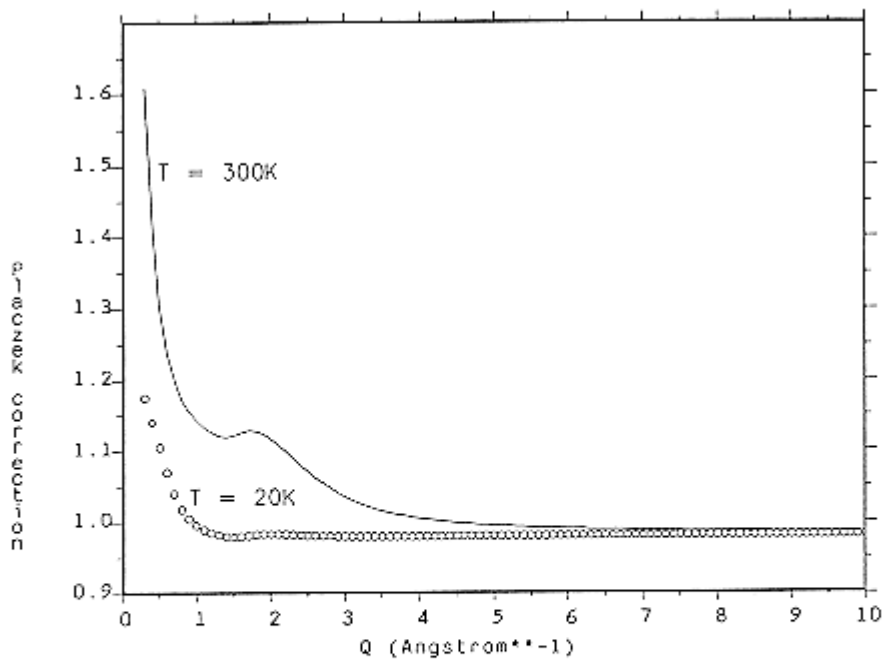
Figure 2.6 Recoil correction for a free deuterium atom at 20K and 300K. The scattering angle is 20°. Note again the large temperature effect at small Q, and that a pronounced structure appears due to the substantial energy transfers that take place in the scattering process.

2.10 Merging the data to form the structure factor

Typically one will record the TDCS at several scattering angles in a TOF diffraction experiment. On SANDALS there are 18 groups of detectors. Which of these groups are to be combined requires a decision by the experimentalist. A typical approach might be as follows:

(a) Correct each angle for inelasticity effects, particularly in the self scattering.
(b) Plot all the spectra on top of each other.
(c) For each group choose a range of Q values over which this spectrum overlaps with at least on spectrum from a neighbouring group at higher or lower scattering angle, and ignore those spectra which clearly disagree with the others. Obviously this is a highly subjective point in the analysis, but if all has gone well with the experiment, it should be fairly obvious where the overlaps occur. The object is to avoid combining different detector banks where there are clearly differences due to say not being able to perform the Placzek correction accurately, such as occurs with light atoms such as deuterium.
(d) Merge the selected spectra over the selected Q range, using the MERGE command.
(e) Finally perform any remaining normalisations as needed such as removing the incoherent scattering and dividing out the scattering cross section. The result should either be in the units of differential cross section (barns per steradian per atom/4π) or have dimensionless units as a structure factor, S(Q).

The merging of spectra is achieved by weighting each spectrum with the intensity with which it was measured. The weighting function is obtained from the corrected intensity data of the vanadium sample contained in the quantity

$$W_j(Q_e) = CAL_V(Q_e) * I_m(k_e) \qquad\qquad 2.10.1$$

Where the suffix j is used to label the j'th group of detectors. Hence if $\Sigma_j(Q_e)$ is the measured differential cross section for the j'th group, the merged differential cross section is obtained by forming the sum

$$\Sigma_M(Q_e) = \left[\sum \Sigma_j(Q_e) * W_j(Q_e) \right] / \sum W_j(Q_e) \qquad\qquad 2.11.1$$

2.11 Analysis to pair correlation function

The inversion of S(Q) data to pair correlation function, g(r), i.e. inversion of equation 1.3.2, can be done by trivial Fourier transform. Routines GTOS and STOG are available to do this, and will allow the inclusion of a window or modification function if needed.

However, such direct Fourier transforms will inevitable lead to spurious structure in the calculated distribution due to the finite extent and statistical noise present in the data. This has been subject to a number of reports, including a preliminary one from the Rutherford Appleton Laboratory by Soper [21], which was presented at the ICANS-X meeting in October 1998. In this alternative method of data inversion, it is proposed to limit the fluctuations in r(g(r) - 1) with increasing r to those that are compatible with the observed width of the peaks in S(Q). In this way the noise and truncation of the data are not reproduced in the simulated pair correlation functions, at the same time that excellent fits to the measured data are obtained.

SECTION 3:

ISOTOPIC SUBSTITUTION NEUTRON SCATTERING METHODS

3 Structure in molecular liquid systems by H/D isotopic substitution neutron scattering methods

3.1 Isotopic substitution neutron scattering

One of the most powerful experimental techniques that can directly probe intermolecular structure in the liquid state is second order difference, isotopic substitution neutron scattering. If the molecular liquid under investigation is water based i.e. as in the study of aqueous solutions, isotopic substitution of the hydrogen sites with deuterium is often the most convenient and most revealing probe of the intermolecular structural correlations. In the case of binary molecular systems where there is a hydrogenous molecular solute species dissolved in water, it is often possible to extract the three intermolecular structural correlations that determine the liquid properties. These three correlations are those between solute molecules, those between solvent molecules and finally between solute and solvent molecules.

In a single neutron scattering experiment, the quantity obtained after the data have been corrected for experimental details such as absorption and multiple scattering of neutrons, the background scattering from the sample cell and the self scattering and inelasticity effects, is the total structure factor $F(Q)$. This is defined as

$$F(Q) = \sum_{\alpha\beta} c_\alpha c_\beta b_\alpha b_\beta S_{\alpha\beta}(Q) - 1 \qquad\qquad 3.1.1$$

where c_α and c_β are the concentrations of atoms of species α and β respectively, whilst b_α and b_β are their coherent neutron scattering lengths. The summation is over all atom pairs in the sample and $S_{\alpha\beta}(Q)$ are the partial structure factors which result from interatomic correlations between atom pairs α and β and where $Q = (4\pi/\lambda)\sin\theta$, the magnitude of the momentum change vector of the scattered neutrons, 2θ is the scattering angle and λ is the wavelength of the incident neutron. These partial structure factors are related to the partial pair distribution functions $g_{\alpha\beta}(r)$ by the mathematical relation

$$S_{\alpha\beta}(Q) - 1 = 4\pi\rho \int r^2 [g_{\alpha\beta}(r) - 1] \frac{\sin(Qr)}{Qr} dr \qquad\qquad 3.1.2$$

where ρ is the average atomic number density of the sample.

It was realized that through the use of isotopes of differing coherent neutron scattering lengths, it is in priciple possible to extract some of the partial structure factors from the total structure factor measured by any single neutron scattering experiment. Provided that the structure of an isotopically enhanced sample is to first order identical, this is a reliable technique.

If two experiments on samples which are identical except for the isotopic composition of one element were performed, a difference between the two total structure factors would result in a composite structure factor containing only interatomic structural correlations involving the substituted atomic species. For example, if a sample consisted of atoms of type A,B and C, the total structural factor of a single experiment would consist of terms in $S_{AA}(Q)$, $S_{BB}(Q)$, $S_{CC}(Q)$, $S_{AB}(Q)$, $S_{AC}(Q)$ and $S_{BC}(Q)$. If the isotopic substitution were performed on atoms of type A and a difference between the two total structure factors taken, the difference composite

structure factor would only contain terms in $S_{AA}(Q)$, $S_{AB}(Q)$ and $S_{AC}(Q)$. This first order difference hence results in a significant simplification of the structural correlations that are to be interpreted.

Now, if a third experiment is performed, again adjusting the scattering length of atoms of type A, this result can be combined with the first order difference information. It then becomes possible to extract a single partial structure factor, $S_{AA}(Q)$. This partial structure factor only contains information relating to interatomic correlations between atoms of type A. This observation forms the foundation on which the technique of second order difference isotopic substitution neutron scattering is based.

In the case of a second order difference hydrogen/deuterium isotopic substitution experiment the total structure factor, $F(Q)$, can be written as consisting of three terms $S_{XX}(Q)$, $S_{XH}(Q)$ and $S_{HH}(Q)$. The label H refers to substituted atoms in the sample and X to unsubstituted atomic species.

$$F(Q) = c_X^2 b_X^2 [S_{XX}(Q) - 1] + 2 c_X c_H b_X b_H [S_{XH}(Q) - 1] + c_H^2 b_H^2 [S_{HH}(Q) - 1] \qquad 3.1.3$$

The composite coherent scattering length, b_X, and concentration, c_X, are defined as

$$b_X = \sum_{\alpha \neq H} \frac{c_\alpha b_\alpha}{c_X} \qquad 3.1.4$$

$$c_X = \sum_{\alpha \neq H} c_\alpha \qquad 3.1.5$$

consequently $c_H = (1 - c_X)$ and the $S_{HH}(Q)$ term in equation 3.1.3 is calculated from

$$S_{HH}(Q) - 1 = \frac{x F_H(Q) + (1 - x) F_D(Q) - F_{HD}(Q)}{c_H^2 \left(x b_H^2 + (1 - x) b_D^2 - b_{HD}^2 \right)} \qquad 3.1.6$$

where the subscripts H and D refer to the experiments upon the hydrogenated and deuterated samples respectively and HD to the mixture sample. x is the fraction of light hydrogen in the mixture sample and thus

$$b_{HD} = x b_H + (1 - x) b_D \qquad 3.1.7$$

From an experimental viewpoint, is should be noted that the maximum difference between the scattering functions can be obtained if the three experiments performed for the second order difference calculation use two pure isotopic compositions and a 50:50 mixture for the third.

The weighted sums for the other partial structure factors in equation 3.1.3, i.e. those that involve unlabelled atoms, are

$$S_{XH}(Q) - 1 = \sum_{\alpha \neq H} \frac{c_\alpha b_\alpha [S_{\alpha H}(Q) - 1]}{c_X b_X} \qquad 3.1.8$$

$$S_{XX}(Q) - 1 = \sum_{\alpha \neq H, \beta \neq H} \frac{c_\alpha c_\beta b_\alpha b_\beta \left[S_{\alpha\beta}(Q) - 1 \right]}{c_X^2 b_X^2} \qquad 3.1.9$$

and these composite partial structure factors can be calculated in similar fashion to $(S_{HH}(Q)-1)$ (see equation 3.1.6).

Using the complemetary Fourier transform relationship to equation 3.1.2, the partial structure factors between atom sites, $g_{\alpha\beta}(r)$, can be calculated for interpretation. The positions of the features in $g_{HH}(r)$ correspond to interatomic distance correlations between substituted hydrogen sites and the area under these features is related to coordination numbers.

The coordination number of atoms of type β at a distance between r_1 and r_2 from atoms of type α is defined as

$$N_\beta^{(\alpha)_{r_1}^{r_2}} = 4\pi\rho c_\beta \int_{r_1}^{r_2} r^2 g_{\alpha\beta}(r) dr \qquad 3.1.10$$

An advantage of the second order difference technique when applied to molecular liquid mixtures is that if the isotopic substitution is performed on atom sites of only one molecular species in the mixture, only interatomic correlations between these substituted sites will contribute to the extracted partial pair distribution function. Hence only intramolecular and intermolecular information from the molecular species that is subject to the substitutions is evident i.e. the technique can be used as a direct probe of intermolecular structure from the viewpoint of the substituted atom sites of the molecule.

3.2 An example of a binary molecular mixture

For binary molecular liquid mixtures, further substitutions are often possible and in combination allow for the extraction of the three aforementioned structural correlations, the solute-solute, solvent-solvent and solute-solvent terms. In total seven isotopically distinct but otherwise identical samples would have to be measured to extract all three of these terms.

An example case for the extraction of the three intermolecular correlations of interest in a binary molecular mixture is the following. A mixture of two molecules with hydrogen sites that are suitable for isotopic substitution is prepared in various isotopic compositions. Labelling the hydrogen sites on molecule 1, H, and those on molecule 2, M, seven experiments need to be performed on mixtures with isotopic compositions indicated by H_H, H_D, H_{HD}, M_H, M_D and M_{HD}. These experiments are

     1. Molecule 1 (H_H) and Molecule 2 (M_H)
     2. Molecule 1 (H_D) and Molecule 2 (M_D)
     3. Molecule 1 (H_{HD}) and Molecule 2 (M_{HD})
     4. Molecule 1 (H_D) and Molecule 2 (M_H)
     5. Molecule 1 (H_D) and Molecule 2 (M_{HD})
     6. Molecule 1 (H_H) and Molecule 2 (M_D)
     7. Molecule 1 (H_{HD}) and Molecule 2 (M_D)

It can be seen that a mixture of experiments 1, 2 and 3 will give the intermolecular correlations between all M and H sites between both molecular species. A combination of

experiments 2, 4 and 5 will give the intermolecular correlations between the M sites only, and a combination of experiments 2, 6 and 7 will give the intermolecular correlations between H sites only.

Obviously if molecule 1 were considered the solvent, and molecule 2 the solute in the mixture, then experiments 2, 6 and 7 give the intermolecular solvent-solvent structural correlations and likewise, experiments 2, 4 and 5 give the intermolecular solute-solute correlations. To extract information on the intermolecular solute-solvent correlations, the total information obtained from experiment 1, 2 and 3 must be combined with the solvent-solvent and solute-solute functions. Labelling the intermolecular solute-solvent correlation ($S_{MH}(Q)$-1), the solvent-solvent correlation ($S_{HH}(Q)$-1), the solute-solute correlation ($S_{MM}(Q)$-1) and the total intermolecular correlation function (from experiments 1, 2 and 3) ($S_{H,M}(Q)$-1), the solute-solvent term can be calculated from

$$c_{H,M}^2 \left\langle b_H^2 \right\rangle \left(S_{H,M}(Q)-1\right) = c_H^2 \left\langle b_H^2 \right\rangle \left(S_{HH}(Q)-1\right) + c_M^2 \left\langle b_H^2 \right\rangle \left(S_{MM}(Q)-1\right) + c_H c_M \left\langle b_H^2 \right\rangle \left(S_{MH}(Q-1)\right)$$

3.2.1

where $<b_H^2>$ is defined as

$$\left\langle b_H^2 \right\rangle = x b_H^2 + (1-x) b_D^2 - b_{HD}^2$$

3.2.2

A subtlety that must be considered in the case of molecular liquid studies is whether in-solution isotopic exchange can occur between substituted sites or between substituted sites and unsubstituted sites. For example in water, hydrogen atoms are free to exchange between water molecules and thus when there is a mixture of light and heavy water, hydrogen and deuterium are free to sites and molecules. If this occurs, the $g_{HH}(r)$ extracted in a second order difference experiment will contain both intramolecular and intermolecular contributions to the structural features. However, if the substituted sites are on non-polar groups such as methyl groups, in-solution hydrogen/deuterium exchange does not take place and when $g_{HH}(r)$ is calculated, only intermolecular terms will contribute. The intramolecular correlations will appear in the $g_{XH}(r)$ and $g_{XX}(r)$ pair distribution functions and are weighted in the composite partial structure factors ($S_{XH}(Q)$-1) and ($S_{XX}(Q)$-1) as

$$\left(S_{XH}(Q)-1\right) = \sum_{\alpha \neq H} \frac{c_\alpha b_\alpha}{c_X b_x} \left(S_{\alpha H}^{\text{inter}}(Q)-1\right) + \sum_{\alpha \neq H} \frac{b_\alpha}{2 N_m c_X b_X c_H} \left(S_{\alpha H}^{\text{intra}}(Q)-1\right) + \frac{(b_D + b_H)}{2 N_m c_H c_X b_X} \left(S_{HH}^{\text{intra}}(Q)-1\right)$$

3.2.3

$$\left(S_{XX}(Q)-1\right) = \sum_{\alpha \neq H, \beta \neq H} \frac{c_\alpha c_\beta b_\alpha b_\beta}{c_X^2 b_X^2} \left(S_{\alpha \beta}^{\text{inter}}(Q)-1\right) + \sum_{\alpha \neq H, \beta \neq H} \frac{b_\alpha b_\beta}{N_m c_X^2 b_X^2} \left(S_{\alpha \beta}^{\text{intra}}(Q-1)\right) - \frac{b_D b_H}{N_m c_X^2 b_X^2} \left(S_{HH}^{\text{intra}}(Q)-1\right)$$

3.2.4

where N_m is the total number of atoms on the molecule and the intra molecular terms ($S_{\alpha\beta}^{\text{intra}}(Q)$ - 1) are defined in the gaussian approximation by

$$\left(S_{\alpha\beta}^{\text{intra}}(Q)-1\right) = \sum_{i=\alpha, j=\beta} \frac{\sin(Q r_{ij})}{(Q r_{ij})} \exp\left(\frac{-Q^2 \sigma_{ij}^2}{2}\right)$$

3.2.5

where the summation is taken only over atoms in the same molecule, r_{ij} is the average separation of atoms i and j and the standard deviation in this mean distance is given by σ_{ij}.

SECTION 4:

THE SANDALS SURVIVAL GUIDE

4 The SANDALS survival guide: a brief introduction to running the SANDALS instrument and analysing the collected data

4.1 Logging on to the SLS Front End Computer

You will run the experiment from the directory:

SLS$DISK0:[SLS]

To log on to the instrument computer, use the username **SLS** and the current password.

To view and analyse the data it is suggested that you use a sub-directory

SLS$DISK0:[SLS.*EXPT_NAME*] , where **expt_name** is chosen by you.

All the files created in the course of the data analysis (but not the raw data files) will be located in this directory. They can then be transferred to your area on the main computer ISISA or elsewhere when the experiment is over. Files left on **[SLS.*EXPT_NAME*]** will be archived and deleted from sls$disk0 approximately one month after the experiment is completed.

The second workstation in the SANDALS cabin, not directly connected to the SANDALS instrument can be used to log on to the ISIS central computer system if you have an account there.

4.1.1 Windows on the SLS front end computer

A common arrangement is to use 4 windows named as follows:

DASHBOARD - the current instrument and run status.

SLS - CONTROL - for running the experiment, from the directory [SLS].

ATLAS - for running ATLAS data analysis programs from the directory [SLS.*EXPT_NAME*]

> To create and use the directory [sls.*expt_name*] on the ATLAS window:
>
> SLS> **create/directory [sls.*expt_name*]**
> SLS> **set def [sls.*expt_name*]**
>
> To verify your location in the computer system:
>
> SLS$> **sho def**
> SLS$> sls$disk0:[sls.expt_name]

GENIE - for running the data display and manipulation program Genie II.

> To set up Genie for [sls.*expt_name*] on the GENIE window:
>
> >> **exit** - if necessary
> SLS> **set def [sls.*expt_name*]**
>
> Then to start Genie type:
> SLS> **GENIE**
>
> Genie header and initialization appears followed by the Genie prompt:
>
> >>

Note Most of the programs detailed below which run under Genie refer to files by run-number and look for them in the default directory. Therefore it is necessary to start Genie from the directory where your files are (e.g. [sls.*expt_name*]). (This does not apply to .RAW files which Genie looks for in the directory [slsmgr.data] by default.)

4.1.2 Using Genie

Full details of Genie operation are contained in the PUNCH GENIE MANUAL [3]. A few useful commands for using Genie are:

>> **a b 1** - 'alter binning to 1' (the default on start-up is to display data in groups of 10 data points).

>> **t mode** - 'toggle mode'. Determines whether data are treated as points or histogram for display.

>> **d/l w***n* *xmin xmax* - displays data in workspace *n* as a line.

>> **d/m w***n* - displays data points with markers.

>> **p/l** or **p/m w***m* - plots data in workspace *m* on the previous displayed graph.

>> **k/h** - creates a plot file of the currently displayed data.

>> **pl2** - sends plot file to laser printer in DAC (R55).

>> **pl4** - sends plot file to laser printer in CRISP instrument cabin.

>> **j/p** - jump out of Genie and restore the command prompt

    SLS>
            without closing Genie. To return to Genie, type:
    SLS> **lo**
    >>

Alternatively, to issue one command line, type:
>> **j**
SLS> Command: **delete file1.dat;*** - (for example)
>>

Do not type **GENIE** *again after using* **j/p** *since this creates multiple Genie processes and eventually may hang up the whole computer!*

>> **exit** - exit and close Genie and return to

SLS>

For more information about printing graphics and text files, type (out of Genie):

SLS> **info laser_printing**

4.1.3 SLS file names

File names for SANDALS data (and other files used in the analysis) are usually made up of 3 parts:

instrument name: **SLS**
run number: **1234** (for example)
ext: **file extension** (file type)

and have the form:

SLS01234.EXT

Some file extensions are:

RAW - raw data files giving counts vs time for each detector
LOG - the sample environment log file created for each run
SUM - data amalgamated into 18 groups as function of Q
MON - incident and tranmission monitor data as function of λ
MUT - total interaction cross-section data as function of λ
AIN - input parameters for calculation of absorption
MIN - input parameters for calculation of multiple scattering
ABS - absorption coefficients as function of θ and λ
MUL - multiple scattering correction
REF - data for vanadium corrections
SMO - corrected and smoothed vanadium data
DCS - differential cross-section for sample
SLF - self scattering of sample (used in some cases only)
INT - interference function (S(Q)) for 18 detector groups
MINT - S(Q) after merging all or chosen detector groups
MOQ - partial structure factor (used in some cases only)

4.2 Running the SANDALS instrument

4.2.1 To start a new run

If the sample or conditions have been changed the run title should be changed first using the CHANGE command:

SLS> **CHANGE**

This enables you to give a run title, user etc, which will be stored with the data.

To exit from CHANGE press F1 (gold) and then E (exit).
Then:

SLS> **BEGIN** begins the run and the screen will respond:

... run 1234 has begun ...

SLS> **@NPCHECK** runs the command file npcheck.com.

NPCHECK has 2 functions:

(i) It ends the run and begins a new run at specified intervals (i.e. after a specified number of microamps, typically 500).
(ii) It checks the neutron/proton ratio (sensitive to instability in the moderator) and compares it with the expected (preset) value. If the value is outside the preset range the data collection pauses for 1
minute and then another check is made. When the ratio is found to be back within the preset range the data collection run is resumed.

The input file containing: the number of microamps, the expected n/p ratio, number standard deviations is **run_par.dat** which should be in directory [SLS.NPCHECK] and can be edited if you need to change these parameters.

Until you exit from the control of a command file by pressing CTRL Y it is not possible to issue commands on the SLS-control window.

4.2.2 To end a run

If NPCHECK (or another command file) is running:

press **CTRL Y**

then type:

SLS> **END**

This ends the current run and saves the data. Terminal responds:

.... data in file SLS01234.RAW....

Notice that the run number on the dashboard is then automatically updated to 1235.

To end the run without saving the data:

SLS> **ABO**

This aborts the current run, data is not saved and run-number is not updated.

To pause the data collection without ending the run:

SLS> **PAUSE** - halts data collection

... make required adjustments ...

SLS> **RESUME** - resumes data collection.

4.2.3 Control of sample temperature

To assign the sample environment block **TEMP1** and/or **TEMP3**, type:

SLS> **cset TEMP1/devspec=***device number* - set device number of sensor
SLS> **cset TEMP3/devspec=***device number* - set device number of sensor
SLS> **cset CAMAC/reset** - dashboard display FALS
SLS> **cset TEMP1/log**
SLS> **cset TEMP3/log**

dashboard display restored.

To control sample temperature:

If for example TEMP1 is the controller, type:

SLS> **cset TEMP1** *required temperature*

To inhibit data collection except when required temperature is reached, type:

SLS> **cset TEMP1/range=***value required temperature*

range is the range in C or K of the ***required temperature*** within which data will be collected if the
control option is on. To switch on the range control, type:

SLS> **cset TEMP1/control**} - sets the control on
SLS> **cset TEMP1/nocontrol** - switches the control off

While the control is on during a data acquisition run and the temperature is out of range, the dashboard will display: **WAITING**.

If TEMP3 is the controller, substitute TEMP3 for TEMP1 in the above.

To see a display of the current temperature control status, type:

SLS> **cshow TEMP1/full** - and/or
SLS> **cshow TEMP3/full**

More detailed information is available from the CAMAC manual or instrument scientists. An example of a command file to run a series of different temperatures is **[slsmgr]repeat_temp.com** .

4.3 SANDALS raw data and detector groups

4.3.1 Raw data files

The 1270 detectors (currently) on SANDALS are in an approximately cylindrical arrangement in rows (see Fig. 1). The raw data files contain the spectra from each of these detectors separately. Spectrum 1 is the incident monitor. Spectrum 2 is the tranmission monitor.
The raw data files are named from the run numbers, for example:

SLS01234.RAW

They are located in the directory

SLS\\$DISK0:[SLSMGR.DATA] which has the **SLS_DATA**

This directory can be searched by typing, for example:

SLS> **dir sls_data:sls0123*.raw**

To inspect a list of runs in the current cycle, including title, date and number of microamps:

SLS> **type sls_data:journal.txt**

The list of runs for a previous cycle, e.g. cycle 94/6, is in the file **sls_data:jour946.txt**.

In many cases it will not be necessary to examine the .RAW files. However, the data can be viewed if necessary. For example in Genie:

>> **ass 1234** - assigns sls01234.raw as the default file
>> **wn=s11** - reads spectrum 11 (detector 11) of sls01234.raw into workspace 1
>> **d w11** - displays counts from detector 11.

Alternatively to plot the counts from a detector without reading into a workspace:
>> **ass 1234**
>> **d s11** - say; displays detector 11
>> **p s12** - say; plots detector 12 on the same graph

See also the data checking routines described in {\bf Section 4.4.3} below.

4.3.2 Detector groups

For most purposes it is more convenient to work with grouped data than with raw data files. The detectors are grouped for data analysis purposes into 18 groups (currently) at a series of angles between 37 deg and 3.5 deg 2θ:

Group 1   20.1 deg
Group 2   18.1 deg
Group 3   16.2 deg
Group 4   14.6 deg
Group 5   13.1 deg
Group 6   11.8 deg
Group 7   9.5 deg
Group 8   7.0 deg
Group 9   5.0 deg
Group 10   3.8 deg
Group 11   31.2 deg
Group 12   27.8 deg
Group 13   24.4 deg
Group 14   21.7 deg
Group 15   36.7 deg
Group 16   33.8 deg
Group 17   31.5 deg
Group 18   29.2 deg

Note 1: Groups 11 to 14 are new detector groups added to the original 10 groups in January 1995 and are in operation from run 8174 onwards.
Note 2: Groups 15 to 18 are new detector groups added in 1998

The grouping of 1270 detectors (currently) into the 18 detector groups is made by the program NORM which is described in **Section(4.5.2)**} below.

The current default grouping of 1270 detectors is defined in the file:-

sls$disk0:[sls]groups_def.dat

For data taken from run 8170 up to August 1995, when SANDALS had 870 detectors in 14 detector groups, the default detector grouping is in **norm_par:groups870_def.dat**
For data taken before run 8170, when SANDALS had 670 detectors in 10 detector groups, the default detector grouping is in **norm_par:groups670_def.dat**.

The (current) default detector group file is **sls$disk0:[sls]groups_def.dat**

4.4 Viewing the data

There are 3 ways of viewing the current data on SANDALS. Of these **SQRAW** is the most reliable because it allows you to check:-

(i) the **level of scattering** against a vanadium standard (which in turn allows you to check for example that the sample cell is filled correctly or has the correct isotopecomposition) and
(ii) the **statistical accuracy** after merging all the detectors.

The only drawback to SQRAW is that it requires you to END the current run and then run PURGE_D/NORM, which can take several minutes. If you require only a quick look at the current data then use either **SQDAE** or **SANQ**.

4.4.1 S(Q) for uncorrected data (SQRAW)

The routine SQRAW provides the best way to check your data before proceeding to do the attenuation and multiple scattering corrections. To run it, type:

>> **SQRAW**

which will run sls$disk0:[slsmgr.aks]sqrawb.com

SQRAW operates on grouped data without corrections for attenuation and multiple scattering and without taking into account the number of sample scatterers in the beam (geometric factors and density)

SQRAW requires as input:

.SUM and .MON for the sample (S) and the background or cell (B)
.SMO and .MON for the vanadium standard (V).

These files must exist in your current directory.

Section 4.5.2 describes how to obtain the .SUM (grouped data) and .MON files, which are created by the program NORM. The vanadium .SMO file calculation is described in **Sections 4.5.5** and **4.5.4**; however, it is likely that you can copy an existing .SMO file to your directory for use in SQRAW
at the beginning of your experiment.)

The incident monitor counts (M) are used to normalize the sample and background counts and an uncorrected S(Q) is calculated for each detector group as follows:

$$SQRAW = \frac{S \times \dfrac{M_v}{M_s} - B \times \dfrac{M_V}{M_B}}{V_{SMO,CORR}}$$

SQRAW creates an output file:

SLS01234.SQRAW

containing the result for each of the detector groups included in the calculation. The last block is the result of merging the data from the groups giving a maximum of 19 blocks (groups 1 to 18 +1). Any resonance regions to be excluded in the merge are input at the start of the routine.

4.4.2 Displaying SQRAW result in Genie

To read a .SQRAW file into Genie for display, type:

>> **@aks0:readall**

and input run number, extension (**sqraw)**, number of groups to be read and a suitable workspace
number for the first group when prompted. If data are in w1 to w19, say, they can be displayed by typing:

>> **d/l w1** - displays data in w1
>> **p w2** - plots data in w2 on same graph as w1
>> **p w3**
.. etc ..

Alternatively, for one group only use the Genie READ command. For example:

>> **read w10 sls01234.sqraw 1**

reads the 1st group in sls01234.sqraw into workspace 10. Then :

>> **d/l w10** - displays the data in w10

>> **read w11 sls01235.sqraw 1** - repeat for a subsequent run
>> **p w11** - compare results for the 2 runs

To specify the range of data displayed in w10 (for example):

>> **d/l w10**
>> **l/x 0 30** for example
>> **l/y 0 3** for example
>> **d**

displays data from 0 to 30Å^{-1} and 0 to 3 units on y axis.
Alternatively,

>> **d/l w10 0 30 0 3** - will do the same.

Fourier transformation of the data in a .SQRAW file is described below in **Section 4.7.1**

4.4.3 Displaying current data from DAE

This can be done using either of the routines SQDAE and SANQ. To run the routine SQDAE type:

>> **SQDAE**

runs sls$disk0:[slsmgr.aks]sqdae.com

When prompted:

input the run number for a vanadium .SMO file (smoothed vanadium data) and select a group of detectors from:

The routine displays the current data divided by the smoothed and corrected vanadium data, as a function of Q. The calculation of the vanadium .SMO file is described in **Sections 4.5.4** and **4.5.5** below. However, if you have not already made the measurement to obtain a vanadium smoothed file for your experiment, it is likely that an existing .SMO file from a previous experiment is available to use.

To run SANQ type:

>> **SANQ**

runs s_p:sanq.com

Input run number for a .RAW file for the vanadium standard data when prompted and select one row of detectors from the menu.

The raw sample and vanadium data are normalised by the sum of their respective monitor counts and the sample data is then divided by the vanadium data. Because it uses fewer detectors, this program produces a display faster than SQDAE does. A .RAW file can also be used for the sample data.

4.4.4 Data checking routines

The following routines can be run to check raw data, detector stability and temperature:

CHECK_RUNS, **PURGE_D**, **FINGER**, **TPLOT** and **SUMSPEC**

4.4.4.1 CHECK_RUNS. Check time, number of microamps and n/p ratio for a run

Type:

>> **@AKS0:CHECK_RUNS**

input run number(s) and make use of HOLD SCREEN key!

4.4.4.2 PURGE_D. Check stability of detectors for a series of runs or an individual run

The routine PURGE_D can be used on all the runs during the experiment to remove noisy, non-functioning or unstable detectors from the data amalgamation process done by the program NORM.

For details on how to run PURGE_D see **Section 4.5.1** below.

4.4.4.3 FINGER. Check a run for noisy or dead detectors

To run the program FINGER, Type:

SLS> **FING**

Then type

fing> **gr norm_par:finger.dat** (defines default grouping of detectors)
fing> **run/nodead 1234** (input required run number)
fing> **begin**

FINGER creates a plot file of the individual detector counts called

sls01234.det

which can be read into a Genie workspace as example above (section (4.4.1.1)) and plotted choosing suitable x and y limits. The x values are detector numbers.

4.4.4.4 TPLOT. Plot time variation of sample temperature (For experiments where temperature is being controlled)

Type:

>> **TPLOT**

input current run or previous run, and a sample environment block (e.g. TEMP1, TEMP3 *in upper case*) when prompted. This routine uses the file **sls01234.log** which is located in the directory sls_data: together with the .RAW files.

4.4.4.5 SUMSPEC. Check counts in each detector

The integrated counts in each detector can also be obtained in an ASCII file by running the program SUMSPEC for a particular run number.

Type:

SLS> **SUM**

Use the menu to set the filename of the .RAW file as required, by typing:
DISK SLS\\$DISK0:
DIR [SLSMGR.DATA]
EXT RAW
RUN 1234

and then type the command
SUM

The results are in an ascii file **scratch$disk:[sls]sls01234.sum** or in **sys$scratch:sls01234.sum** if you are logged on under another username. This file is **not** to be confused with the (binary) file output sls01234.sum containing the data as a function of Q which is created by the program NORM.

4.5 Data analysis

The steps in the data analysis needed to obtain the total differential cross-section (eqns.1.2.4 to 1.2.6 in ATLAS manual) in a simple case are as follows:-

1. **Obtain a detector groups file (PURGE_D)**

2. **Grouping of raw data (NORM)**

3. **Calculation of attenuation coefficients and multiple scattering for sample+cell, cell and vanadium (CORAL)** (Eqn. 2.5.1 in ATLAS manual).

4. **Vanadium standard data correction and smoothing (VANSLS)**
(Eqn. 2.7.6. in ATLAS manual).

5. **Calculation of total differential cross section for sample (ANALYSE)**
(Section 2.8 in ATLAS manual).

This includes:
Application of attenuation and multiple scattering corrections to sample and cell(s)
Subtraction of background and cell scattering
Normalization of sample scattering by volume, density and vanadium standard.

Step 5 creates a file **SLS01234.DCS**

containing the differential cross-section for each detector group. To obtain the final S(Q) for the sample, 2 further steps are required:

6. **Subtraction of single-atom scattering** (eqn. 1.2.15 in ATLAS manual).

7. **Merge S(Q) from all or selected detector groups (MERGE_SLS)**

4.5.1 PURGE_D: selection of detectors to be used in NORM

The detector groups file tells NORM which detectors are to be included in the data amalgamation. **PURGE_D** enables you to create your own detector groups file **sls01236.grp** on the basis of the performance of the detectors during your experiment. The program removes noisy and unstable detectors from the default detector groups file after checking a set of .RAW files (or one .RAW file) from the same sample.

The set of runs to be compared must correspond to the same sample under the same conditions.

To use PURGE_D, first copy the default detector groups file to the filename **groups_def.dat** in
your area. The correct default file for the currently installed detectors is **sls$disk0:[sls]groups_def.dat**.

To copy this file to your current area, type:

SLS> **copy [sls]groups_def.dat groups_def.dat**

The groups_def.dat you use must correspond to the detectors installed at the time of your experiment. (For example, use **norm_par:groups870_def.dat** for data taken before August 1995 (870 detectors) and **norm_par:groups670_def.dat** for data taken in 1994 before run 8174.

To run PURGE_D for a set of runs, type (within Genie)

>> **PURGED**

(or if *not* logged in under SLS username, type:

>> **@AKS0:PURGE_D**

The program **SUMSPEC** (giving the counts in each detector) has to be run for each .RAW file which is to be used in PURGE_D, before the main part of the routine can be run. SUMSPEC can be run from within PURGE_D by answering {\bf 1} to the first question. For details on using SUMSPEC see above **Section 4.4.3.5**.

When prompted, input the run numbers of the .RAW files to be compared and two values for the detector stabilities required over the series of runs. Suggested values to input for the required stabilities are:
0.1 0.02

These values mean that 10% variation in counts is allowed for an individual detector over the series of runs and 2% variation in the total counts from all the detectors is allowed over the series of runs.

If only one run is being checked, the program looks for noisy and quiet detectors and the acceptable level of counts for each detector is set within the program.

You may require greater detector stability, in which case you can use lower values than those suggested above. However, if you input too small a value for the stability of the individual detectors some detectors may be removed purely because the statistics are poor. This problem can be exacerbated if the sample is a weak scatterer, in which case you may need to *increase* the values of the stabilities requested.

The detector groups file is output in the local directory, called:
SLS01236.GRP
where 1236 is the last run-number of the set of runs input to the routine.

It is suggested that PURGE_D is used iteratively on each set of runs during the experiment. The final sls01239.grp can then be used for the data analysis.

PURGE_D accumulates a list of bad cells over the series of iterations in a file called **bad_det.dat**, which lists all the spectrum numbers of the bad detectors found. The value of -1 or -2 against a spectrum number indicates whether the detector was out of range (-1) or fluctuated too much (-2).

The bad cells found in any particular run are output in an ascii file called **sls01234.bad** which has the same format as bad_det.dat. A plot file is also created, called **sys$scratch:sls01234.dif**, which can be read into Genie for display using the command

>> **load wn sys$scratch:sls01234.dif aks0:readdif**

The x values on the plot are spectrum numbers 1 to 1270.
Note: Currently spectra 3-10 and 651-670 should have no data in them.
Note: If one run is discarded by PURGE_D because of a large number of malfunctioning detectors, you will need to re-set the file bad_det.dat before running PURGE_D again. This can be done by copying the last sls01234.bad (from your *previous* set of runs) to the file name bad_det.dat.

To use the detector groups file created by PURGE_D in NORM, input the filename **sls01236.grp** when prompted (instead of the default file norm_par:groups.dat).

4.5.2 Running NORM

NORM is run in batch using the A_B (ATLAS batch) menu:

SLS>**A_B** - gets the menu

select **1** for **NORM**

answer questions (defaults can be used normally) and input run number(s) when prompted.

NORM operates on one or several .RAW files.   The Q value for the counts in each detector is calculated using the data on flight-path and angle for each detector contained in the file:

sls$disk0:[slsmgr.tables]:detector970.dat .

Two output data files are created:

(i) **SLS01234.SUM** containing the summed counts as a function of Q for each detector group (file contains 18 blocks)

(ii) **SLS01234.MON** containing the incident monitor spectrum (block 1) and the transmission monitor spectrum (block 2), both as a function of λ.

By default the routine uses the information on detector groups contained in:

norm_par:groups.dat

but this default file should not normally be used.

The routine **PURGE_D** should be used to create a current detector groups file **sls01234.grp** from which bad detectors have been removed (see **Section 4.5.1** above) before running NORM.

The .SUM and .MON files can be read into Genie and displayed as described in Section 4.4.1.1. above.

Note: No normalization to the incident monitor counts has been done at this stage.

4.5.3 Attenuation and multiple scattering (CORAL)

4.5.3.1 .MUT files

The calculation of attenuation and multiple scattering factors requires data on the wavelength-dependent total interaction cross-section for the sample, cell and vanadium:

$$\sigma_T(\lambda) = \sigma_S(\lambda) + \sigma_A(\lambda) \qquad\qquad 4.2$$

contained in files with the extension .MUT . See ATLAS Manual section 2.4(b).

A transmission monitor is now installed on SANDALS and transmission data can be used to obtain the .MUT files. Alternatively, files containing the cross-section data for your sample can be created from tables (and from existing transmission data for H and D) as described in section 4.5.3.3 below.

4.5.3.2 .MUT files from transmission monitor data

See also ATLAS Manual section 3.7 for details of the routines to calculate .MUT files from transmission data. To use these routines the .MON files for the relevant sample, container, vanadium and background must be in the current directory.

In flat-plate geometry, use the routine **s_p:tfm.com** by typing:

>> **@S_P:TFM**

whilst for cylindrical geometry, one uses **S_P:TCM.COM**

and input sample and background numbers when prompted. The routine uses the ratio of the transmission data (block 2 of .MON file) from sample and background, fits a polynomial to the result and creates a .MUT file

sls01234.mut

Typical values to try for the order of polynomial for the fit are between 1 and 4.

Note: If the sample is in a container, the ''background'' data used should be the data from the container, not the data from the empty instrument.

4.5.3.3 Calculation of MUT data files for samples

The output .MUT file is essentially the result of using equation (4.2) over a suitable range of wavelengths for the experiment (by default 0.15 to 6.45Å).

The method to choose depends on the composition of your samples. If no component in the sample has a wavelength-dependent scattering cross-section (usually meaning it does not contain H or D) the .MUT file can be easily calculated by method (a) (MUT0). If any component in the sample has a wavelength-dependent scattering cross-section, use method (b).

(a) Samples for which the scattering cross-section σ is independent of wavelength for all components (MUT0)

This will apply to most samples except those containing H or D. The sample can consist of one or several elements or isotopes. Type:

>> **@G_F:MUT0**

and when prompted input a workspace number for the result and select option:-
1 sample contains natural elements only or **2** some component of the sample is isotopically enriched.

When prompted, input the chemical symbol and the number (or fraction) of each component in the sample. If you select the `isotopes' option you are then prompted to input the mass number and the fraction of each isotope for the isotopically enriched element. (By default the program uses a table
of cross-section data from the 1991 compilation of V.F. Sears.)

The resulting cross-section data is put into the chosen workspace (say w1) and can then be displayed by typing (in point plotting mode)
>> **d/l w1**

To create a file of the result, type:
>> **aa**

then input a suitable name
(e.g. SAMPLE1) when prompted and the file (e.g. SAMPLE1.MUT) will be created. This is an ASCII file and can be inspected to check that the value of the total cross-section at 1.8Å is sensible.

Note. The total cross-section values calculated by MUT0 are given *per atom*.

.MUT files for various samples already exist available for use. See sections **4.5.3.4** and **4.5.3.5**
for how to combine and rename these files for your sample, if required.

(b) Samples containing some component(s) with a wavelength-dependent scattering cross-section σ.

Usually this means samples containing H or D, and water.

In this case you can use existing .MUT files for H, D, H_2O and D_2O which are the result of experimental measurements. These can be combined with .MUT files calculated from tables as required for your sample **Section 4.5.3.5** below. For this you can use existing (calculated) files or else create new files calculated using MUT0 as described in **(a)** above, if required.

.MUT files for the following samples exist in the directory:

sls\$disk0:[slsmgr.aks] (logical name **aks0:**)

which can be inspected by typing:

>> **dir aks0:*.mut**

H_2O (molecule)
D_2O (molecule)
null water (molecule)
deuterium
hydrogen
lithium
carbon
nitrogen
oxygen
sodium
sulphur
chlorine
silicon
vanadium (van.mut)
titanium-zirconium alloy (tizr.mut)

Notes
(i)   The first 5 files are derived from experimental measurements on water. The others are derived from cross-section tables.
(ii)   The values given are *per atom* except those for water which are *per molecule*.

4.5.3.4 To copy and rename existing .MUT files

To use one of the files existing on aks0: for your experiment, e.g. for the vanadium run, you can copy and rename it by typing:

SLS> **copy aks0:van.mut sls01236.mut**
and to verify, then type:
SLS> **dir sls01234.mut**
and terminal responds
Directory SLS\\$DISK0:[SLS.*EXPT_NAME*]
SLS01234.MUT
Total of 1 file

.MUT files can be read into Genie and plotted by typing:

>> **load w1 atom.mut g_f:readcs** - read atom.mut
>> **t mode** - select point-plotting mode since file is not histogram
>> **d/l w1 0 7** - plot cross-section data up to 7 Å in λ.

See following page for how to combine .MUT files.

4.5.3.5 To combine .MUT files using Genie:

\>> **lo w1 atom1.mut g_f:readcs**}
\>> **lo w2 atom2.mut g_f:readcs**}
\>> ...   etc. ...

add appropriate multiples (or fractions) of atom1.mut, atom2.mut .. as required for your sample:

\>> **wn = N$_1$*w1 + N$_2$*w2 + ...**

to get cross-section per atom (if required), divide by total number of atoms N :

\>> **wn = wn/N**

optionally, plot result in wn to check that the value at 1.8Å is sensible :
\>> **d/l wn**

then write out wn to new file sls01234.mut :

\>> **function wn aks0:writework wn**

enter name: **sls1234.mut**
histogram form?   **0** (data not in histogram form)

As an example, to create a .MUT file for a sample of NaCl in D$_2$O , you could read into Genie and combine the following 3 files:

aks0:sodium.mut, **aks0:chlorine.mut**, **aks0:D2O.mut**. Optionally, the files could be copied to your directory first (see previous page).

4.5.4 Running CORAL

NB. CORAL requires that the .SUM and .MUT files for the relevant samples are in your current directory.

4.5.4.1 CORAL input

SLS> **CORAL**
puts the user into the CORAL environment with prompt
c>

Then type:
c> **set dir [sls.*expt_name*]**
c> **set ext SUM**

to set the default directory and file extension. (If you are not working on SLS it may also be necessary to set the default **disk** and **inst**)

c> **run 1234** - set run-number of appropriate sample
c>**begin**

and input the information requested.
Input required is:
dimensions
absorption cross-sections
number densities

(See below **Section 4.5.4.5** for values for vanadium and titanium-zirconium alloy. Absorption and number density values can be calculated for composite samples using the program CROSS **Section 4.5.4.6** below.)

Note 1: For cylindrical geometry the beam dimensions are required:
Beam height=3.2cm
Beam width =3.2cm
(beam area is 3.2cm diameter disk).

As of October 1994, horizontal and vertical variable beam aperture jaws have been installed, which can be used to reduce the beam dimensions if required (e.g. for narrow flat-plate samples).

Note 2: Coral can now be run from the A_B menu as option 11, which is makes life much easier and precludes the need to set up disk, directory, instrument and extension.

4.5.4.2 CORAL output

CORAL allows you to calculate either absorption corrections (A) or multiple scattering corrections (M) or both for the sample in question. You select which you require and files containing the relevant parameters:

sls01234.ain (absorption)
and/or
sls01234.min (multiple scattering)

are created and used as input to the batch job which calculates the corrections. The command files
to run the batch job are also created and are:

abs01234.com
and/or
mul01234.com

The job submitted by CORAL outputs the absorption and multiple scattering correction files, for example:

sls01234.abs (absorption correction)
sls01234.mul (multiple scattering correction)
sls01236.ref (vanadium corrections)

It is unwise to run CORAL again to create another .ABS or .MUL file before the previous job has finished running because this can cause confusion between intermediate files.

If not running from A_B to exit from CORAL, type:
c> **exit**
SLS>
 - or
c> **j/p** to leave the process temporarily; to return to it, type:
SLS> **lo**
c>

4.5.4.3 What output is required for the experiment?

In a simple case of an experiment involving measurements on the following ''samples":

(i)   sample in cell (S+C) or sample alone (S)
(ii)   empty cell (C) (if any)[*]
(iii)   vanadium standard (V)
(iv)   background (B)

CORAL should be run for the following cases:

(i)   "sample"= **S+C** or **S**; requires **.ABS** and **.MUL**
(ii)   "sample"= **C**; requires **.MUL**
(iii)   "vanadium".   An input parameter file .MIN is created and the output vanadium corrections file is named **.REF**.

Note. At the beginning of CORAL you select whether you wish to calculate the corrections for a "sample" or for "vanadium" data. For the multiple scattering corrections on an empty cell ((ii) above) select "sample". Then treat the cell material as a sample alone (e.g. 2 cell walls of 0.1cm each are treated as a sample 0.2cm thick).

[*]Obviously "cell"may in practice mean several layers of material around the sample, such as a furnace, radiation shield, etc. in addition to the sample container. See earlier chapter of the ATLAS manual for more details.

4.5.4.4 Submitting jobs directly

It may sometimes be convenient to edit a AIN or .MIN parameter file and submit the job to calculate the correction factors outside CORAL.

To submit the ABS01234.COM or MUL01234.COM file, type:

SLS> **@g_f:sub abs01234 sls$batch** or
SLS> **@g_f:sub mul01234 sls$batch**

Note.   When running under username SLS you have access only to SLS$BATCH. However, if you are running under your own username SLS$BATCH can be replaced by any batch queue in the command above, e.g. SYS$BATCH).

4.5.4.5 Parameters for vanadium, ti-zr cells and beam

Usable values for absorption and number density for vanadium and ti-zr (as in the standard SANDALS sample cells) are as follows:

vanadium
σ_A (1.8Å) = 5.080 barns
ρ = 0.07210 Å^{-3}.

ti-zr alloy
σ_A (1.8Å) = 4.12 barns
ρ = 0.0542 Å^{-3}.

Usable dimensions for the standard vanadium slab and the standard flat ti-zr cells are as follows (users may wish to check these where possible):

vanadium slab
width = 5.0 cm
thickness = 0.348 cm
(vanadium slab is 5.0 cm x 5.0 cm square)

ti-zr flat cell ("new" wide cell)
internal width (sample) = 3.5 cm
external width = 3.8 cm
wall thickness = 0.11 cm (each wall)

ti-zr flat cell ("old" narrow cell)
internal width = 2.0 cm
external width = 2.2 cm
wall thickness = 0.10 cm (each wall)

beam dimensions
Beam height=3.2cm
Beam width =3.2cm
(beam area at sample is 3.2cm diameter disk).

As of October 1994, rectangular variable beam aperture jaws have been installed, which can be used to reduce the beam dimensions if required (e.g. for narrow flat-plate samples).

4.5.4.6 Absorption and scattering cross-sections for samples of more than one atom type (CROSS)

Absorption and scattering cross-sections (also atomic weights, atomic fractions, number densities and coefficients of partial pair correlations) for composite samples can be calculated using the program **CROSS**. Type:

SLS> **cross**

and input information on the sample composition when prompted. An output file containing the data is created:

sample_name.**xsect**

where sample_name is chosen by the user. This file can be printed by typing:

laser2 sample_name.xsect (laser printer in DAC R55)

or

laser4 sample_name.xsect (laser printer in CRISP cabin).

4.5.5 Vanadium data correction and smoothing (VANSLS)

4.5.5.1 Input and output

To run VANSLS the following data files must be in your current directory:-

for **Vanadium : .SUM, .MON and .REF**
for **Background : .SUM and .MON**

This routine corrects the vanadium data and smooths the data for each detector group by fitting to a theoretical spectral shape. The corrected counts are normalised by the number of vanadium scatterers in the beam using the vanadium and beam dimensions and vanadium number density input in CORAL. The corrected, smoothed vanadium data is output in a file named:

SLS01236.SMO

The routine VANSLS can be run either in batch or interactively.

4.5.5.2 Batch running

In this case use the ATLAS batch menu. Type:

SLS> **A_B**

Select **2** for **VANSM**

then input whether cylindrical rod or vanadium plate is being used, run numbers for vanadium and background and other parameters as prompted.

Typical values used are: Temperature=300K, Q-bin width=0.05 Å^{-1}. For the case of a flat plate vanadium sample an additional question is asked; see **Section 4.5.5.3 (b)** below.

The residuals from the fit for each group are written to a file **sls01236.rsd** which can be read into Genie and displayed.

4.5.5.3 Interactive running

Alternatively, you can run the routine interactively in Genie, in which case you can see what is going on and get plots of the fit for each group.

The method of running interactively depends in whether you are using a flat vanadium plate or a cylindrical rod.

(a) Cylindrical Geometry

Type in GENIE:

>> **@s_p:vansls**

and input information when prompted.

Note. The files **spectrum001.dat** ...**spectrum018.dat** will probably not be in your directory the first time you run the program; on answering **1** (=no) the files will be copied to your directory. (These files are located in the directory **s_p:**)

(b) Flat Plate Geometry

Type in GENIE:

>> **@s_p:vanslab**

and input information when prompted.

Notes:

(i) Typical values used are: Temperature=300K, Q=bin width=0.05 $\mathrm{\AA}^{-1}$}.

(ii) The files **spectrum001.dat ...spectrum018.dat** will probably not be in your directory the first time you run the program; on answering **1** (=no) the files will be copied to your directory. (These files are located in the directory **s_p:**.)

(iii) Lateral width of vanadium slab= 0.5 x (width) x ρ_V.
Values of width (cm) and ρ_V (scattering centres per $\mathrm{\AA}^{-3}$.) for the standard SANDALS vanadium slab are given in **Section 4.5.4.5** above.

4.5.6 Differential cross-sections (ANALYSE)

4.5.6.1 ANALYSE input and output

This routine requires that the following data files are in your current directory, named by the appropriate run-numbers: -

S + C (or **S**) : .SUM, .MON, .MUT, .ABS, .MUL

C : .SUM, .MON, .MUT, .MUL (if cell(s) used)

B : .SUM, .MON

V : .SMO, .MON, .MUT

ANALYSE normalizes the counts from sample, cell and background by the incident monitor spectrum, applies the corrections for attenuation and multiple scattering and subtracts the background and corrected cell counts (if cell(s) used). The sample counts are normalized to units of barns using the corrected vanadium data (.SMO).

The output from ANALYSE is a file named from the sample run number:

SLS01234.DCS

The .DCS file contains the differential cross-section for each detector group separately, in 18 blocks. These can be read into Genie and plotted as indicated above in **Section 4.4.2**.

Refer to **Section 4.7.1** for how to calculate the Fourier transform of the DCS data.

4.5.6.2 Running ANALYSE

The algorithm for calculating the differential cross-section is described in detail in the ATLAS manual section 2.8, with a summary in section 3.10.

ANALYSE should be run *only* from the ATLAS Batch menu, by typing:

SLS>**A_B**

select **3** for **ANALYSE** from menu

then select either cylindrical (C) or flat-plate geometry (F is default). Input run numbers and other parameters when prompted. The following 3 files are created for running the batch job:

sls01234.anab_com - This is the command file running the batch job.

**scratch$disk:[sls]sls01234.anab_log -**This is the job log file created on scratch$disk:[sls] (or on sys$scratch if you are not working on SLS).

sls01234.anab_dat

This file contains the run numbers and other parameters you have input. The A_B ANALYSE routine includes the option to re-use an existing sls01234.anab_dat file. So if you need to run ANALYSE again on the same sample you can edit this file if necessary and then choose the option to re-use it.

The geometric input parameters are defined as follows, depending on whether you are using cylindrical or flat-plate geometry:-

(a) Cylindrical Geometry

"sample calibration constant" = (beam height) x πr^2 x ρ_S

where r is sample radius (cm) and ρ_S is sample number density (scattering centres per Å^{-3}.). See Section 5.4.5. above for beam dimensions.

(b) Flat plate geometry

Unless told otherwise (see definition of XFRAC below) the program assumes that both sample and vanadium have a cross-sectional area the size of the beam (3.2 cm diameter). The thickness of the
vanadium slab (t_V.) is taken account of in the vanadium corrections file SLS01236.REF. This dimension is therefore included in the calibration file SLS01236.SMO which represents the normalization per unit area of the sample data.

Input parameters for flat-plate geometry are:

(i)   **"sample calibration constant"** = t_S x ρ_S,

where t_S is sample thickness (cm) and ρ_S is sample number density (scattering units per Å^{-3}.).

See **Fig. 4.2a** for relevant geometry.

(ii)   **"Lateral width of sample"** = 0.5 x W_S

where W_S is width of sample (cm). (See Fig. 2a).

This factor tells the multiple scattering routine the region of sample *outside the beam area* where multiple scattering could occur.

(iii)   **"Lateral width of cell"** = 0.5 x W_C

in analogy with (ii) above (Fig. 2b).

(iv)   **"Fraction of sample in the beam"**, XFRAC, is defined as the ratio:

$$\text{XFRAC} = (\text{area of sample in beam}) / (\text{area of beam})$$

if the sample area is less than the beam area. Otherwise, XFRAC = 1. This factor is needed because the sample counts are normalized by the volume of vanadium in the beam. Therefore the vanadium scattering has to be reduced by a factor if the area of the sample in the beam is less than the area of the vanadium slab in the beam. See **Fig. 2c**.

4.5.7 Self-scattering correction (SUBSELF)

Note. If the experiment is to obtain the partial structure factors using H/D substitution on 3 isotoptically distinct samples, the self-scattering correction forms part of a series of routines described below in **Section 4.6.1**.

The routine SUBSELF calculates the self-scattering by fitting a low order Chebyshev polynomial to the differential cross-section for each detector group in the .DCS file. The self-scattering is then subtracted from the data in the .DCS file. The resulting interference function for each group is written out to a file named:

SLS01234.INT

which can be read into Genie using the READ command or @aks0:READALL and plotted as described in Section 4.2 above.

To choose the appropriate order of polynomial without creating an output file, type:

>> **@s_p:subselfdemo**

This routine allows you to compare visually the fits to the differential cross-section for different detector groups, choosing various orders of polynomial (suggested values to begin with are between 2nd and 5th order).

Notes:
(i) Any resonance regions in the data which should be ignored in the fit can be input at the start of the routine.
(ii) The polynomial should not fit the sharp (interference) structure in the data. For this reason the routine reduces the order of the polynomial as the Q range of the data is reduced at the lower detector angles (higher detector groups). This is done automatically in SUBSELF after the user has chosen the order for the ''initial fit'' i.e. for the highest angle group.
(iii) The ''minimum radius for g(r)'' is used to calculate a correction to the fitted polynomial. This is done by Fourier transformation of low-r structure below the minimum radius (minimum interatomic distance) you have chosen (e.g. 0.5Å).

When you have decided on a satisfactory initial order of polynomial and "minimum radius" to use in the fit and wish to create the output file, type:

>>**@s_p:subself**

4.5.8 Calculation of S(Q) (MERGE_SLS)

This routine makes a weighted average of the data from all or selected detector groups in the .INT file. You select which groups are to be included and the lowest and highest Q value to be included in the merged data.

To decide which groups are to be merged, the consistency between the different detector groups in the .INT file can be examined in Genie. For example, type:

>> **@aks0:readall**

read in all groups in sls01234.int into workspaces 1 to 18 (say) then :

>>**d/l w1**
>>**p w2**
>>**p w3**
>>**p w4**
... etc ...

To use MERGE_SLS, type:

>> **@s_p:merge_sls**

and input run-number and extension (usually .INT) of file to be merged, extension (usually .MINT)
of merged output file, group numbers to be merged and Q limits when prompted.

Fourier transformation of the merged S(Q) in sls01234.mint to obtain g(r) is described in **Section 4.7** below.

4.6 Calculation of partial structure factors using H/D substitution

The series of routines to calculate the partial structure factors (HH, XH and XX) from the differential cross-sections for 3 samples should be run ONLY in batch mode using the ATLAS batch menu. The interactive versions will not be maintained in future.

To do this, type:

SLS> **A_B**

and select **7** for **H/D substitution** from menu.

Input run numbers for the .DCS files for the 3 samples (hydrogenous, deuterated and a mixture) and other sample information when prompted. This input information is written to a file in your local directory (e.g.[SLS.*EXPT_NAME*]:

sls01235.hdb_dat

where 1235 is the run number of the mixture sample. This file can be edited and/or re-used if required next time you call the **H/D substitution** routines from the ATLAS Batch menu.

Three other files are also created for running the batch job:-
sls01235.hdb_com is submitted to run the batch job
sls01235.hdb_log is the job log file (created in scratch$disk:[sls] or in sys$scratch if you are not working on SLS)
sls01235.hdb_run is a command file that executes a series of 4 Genie routines:-
CALCSELF3, **SUBSELF3**, **MERGE_SLS** and **PARTIAL**.
These routines are described in the following sections.

The output data files from **H/D substitution** are:

SLS01235.SLF the self scattering function (18 groups)
SLS01234.INT, SLS01235.INT, SLS01236.INT the interference functions for the 3 samples (18 groups in each file)
SLS01234.MINT, SLS01235.MINT, SLS01236.MINT S(Q) for the 3 samples after merging data from all or some of the 18 groups
SLS01235HH.MOQ HH partial structure factor
SLS01235XH.MOQ XH partial structure factor
SLS01235XX.MOQ XX partial structure factor

4.6.1 Self-scattering function (CALCSELF3)

The routine CALCSELF3 uses a linear combination of the differential cross-sections from the 3 samples (deuterated, hydrogenated and a mixture) to make an estimate of the average single atom scattering for the system [A.K. Soper and A. Luzar, J. Chem. Phys., **97** 1320 (1992)].

The output is a file containing the fitted self-scattering function for each detector group, named:

SLS01235.SLF

1235 is the run-number for the mixture sample.

Only one self-scattering file is needed for the 3 samples.

<u>**Notes**</u>

(i) "Order of polynomial for initial fit":
The routine currently fits to the log of the data as a function of energy. A typical value to try for the order of polynomial is 1,2 or 3.
(ii) The "minimum radius for g(r)" is used to calculate a correction to the fit as described above for SUBSELF (Section 5.6). Suggested value to try is between 0.5 and 1.0 Å.
(iii) The order of polynomial and minimum radius should be chosen to fit the underlying shape of the data but without fitting the interference structure.

There is also a demonstration version of CALCSELF3 which allows you to do some trial fitting without creating an output file. To use this, type in Genie:

>>**@s_p:calcself3demo**

4.6.2 Subtraction of self-scattering (SUBSELF3)

SUBSELF3 has to be run for each of the differential cross-section files (.DCS) for the 3 samples. The routine subtracts a suitable fraction of the self-scattering function (.SLF), multiplied by a correction function, from the data in each of the detector groups of the .DCS file.

The resulting interference function for each detector group is written to a file named:

SLS01234.INT

Usually the values for order of polynomial and minimum radius needed for the fit in SUBSELF3 are lower than those used for CALCSELF3. Normally the order of polynomial required is 1 or 2.

There is a demonstration version of SUBSELF3 which allows you to do some trial fitting without creating an output file. To use it, type in Genie:

≫**@s_p:subself3demo**

4.6.3 Merge detector groups (MERGE_SLS)

MERGE_SLS allows you to merge all or selected detector groups from the .INT file for a sample as described in detail in **Section(5.8)** above to produce the S(Q) file (.MINT). This has to be carried out for each of the three samples.

4.6.4 Calculation of partial structure factors (PARTIAL)

The partial structure factors are calculated from the S(Q) (.MINT files) for all 3 samples.

Three files are output, containing the $S_{HH}(Q)$, $S_{XH}(Q)$ and $S_{XX}(Q)$ and are named:

SLS01235HH.MOQ
SLS01235XH.MOQ
SLS01235XX.MOQ

1235 is the run number of the mixture sample.

4.7 Calculation of g(r)

4.7.1 Genie routine STOG

Genie routine STOG (transforms S(Q) to g(r)) can be used to Fourier transform data in a workspace. The routine requires that the data to be transformed is asymptotic to 1.0 .
To carry out a F.T. on the output of SQRAW or on one group of the differential cross-section data for example:

>> **read w1 sls01234.dcs 1** - read block 1
>> **d/l w1**
>> **cu** - use cursor to find asymptotic level of data
>> **w1=w1/*level*** - divide by value of asymptotic value to get new level at 1.0 and optionally plot again to verify:
>> **d w1**

To call routine STOG, type:

>> **transform w1 g_f:stog w2** (**tr** is sufficient)
Input maximum distance in r space (e.g 10 Å)
Input number of points in r space (e.g. 500)
Select whether or not a window function is used on the input data:

....output is in point mode ...

>> **t mode** - unless already in point plotting mode \\
>> **d/l w2 0 10**

To Fourier transform the merged interference function .MINT, which is asymptotic to zero, translate the data by 1.0 before calling STOG:

>> **read w1 sls01234.mint**
>> **w1 = w1 + 1.0**

It is sometimes useful to reduce the range of data in w1 before transforming:

>> **read w1 sls01234.sqraw 19** - read block 19 (merged groups)
>> **d/l w1**
>> **rebin w1 0.5 : 30.** - reduce range of data to 0.5 - 30 Å^{-1}

4.7.2 MDGOFRSHELL

MDGOFRSHELL is a Fourier transform program for S(Q) data which attempts to generate a pair correlation function g(r) which is as smooth as possible (least noisy) but consistent with the diffraction data.

There is a detailed set of instructions in the directory **aks0:** together with files required to run the program, which can be copied to your directory.

To print the instruction notes:

SLS> **laser2 sls$disk0:[slsmgr.aks]user_notes_mdg.txt**

Alternatively use **laser4, laser1** etc.

4.8 Data analysis on ISISA

Users are "discouraged" from continuing to use the SLS computer for data analysis after the end of the SANDALS experiment. You can get a user account on ISISA by contacting Computer Support in room 1.37 on 1st floor of R3, ext. 5415, email SUPPORT. Mobile phone numbers: 3029 (internal), 0585 286687 (external).

4.8.1 Access to SANDALS programs

All the routines available on SLS can be used on ISISE but you will need to set up some directory names on your own area in order to be able to access them. The easiest way to do this is to copy the relevant command lines from the file [SLS]LOGIN.COM to your login.com or to a separate
command file.

The command lines you need are:-

$@lad$disk:[ladmgr.progs]atlas_logs
$ ass sls$disk0:[slsmgr.aks] aks0
$ ass sls inst_name
$ ass sls inst_abrv_name
$ ass sls$disk:[slsmgr.tables] norm_par
$ ass sls$disk:[slsmgr.genie]genieinit.com genieinit

4.8.2 Restoring data from archive

4.8.2.1 Raw data files (.RAW)

During the experiment the raw data files (.RAW) are stored in the area sls$disk0:[slsmgr.data] but they are archived onto optical disk and then deleted from sls\$disk0 regularly. The routine **RESTSLS** restores raw files to the area scratch$disk:[slsmgr.data] where they will remain for a week before being deleted. This area has the logical name sls_data so that the SANDALS programs such as NORM access the restored files there automatically.

To use RESTSLS, type:

$ **RESTSLS**

and input the first and last run-numbers to restore when prompted. This routine is especially useful because a number of runs can be restored without specifying all the run numbers separately.

If you need to restore a raw data file without the help of RESTSLS, you can use the command:

$**restodsr/cat=sls$disk:[slsmgr]catalogue.946**
/out=scratch$disk:[slsmgr.data]sls01234.raw [slsmgr.data]sls01234.raw

where **946** refers to the cycle number during which the data were collected (cycle 94/6 in this example).

To check that your files are in the restore queue, type:

$ **manodsr/list=r**

4.8.2.2 Data on user area of SLS computer

Any files that you leave on your area sls$disk0:[sls.*expt_name*] after the experiment is over are likely to be archived in the SLSMGR area and deleted from the SLS disk within a month. Therefore it is a good idea to copy all the files you want to keep over to your ISISE account or elsewhere and archive them if necessary (type HELP OPTICAL for more information on the archiver). Please see the instrument scientist if you need to restore files from the SLSMGR archive.

4.9 Figures

Figure 1. The SANDALS diffractometer.

Figure 2. Definition of dimensions used in input to ANALYSE (Flat plate geometry)

(a). Shows the definition of sample thickness (t_S) and sample width (W_S).

(b). Shows the definition of cell thickness (t_{C1} and t_{C2}) and cell width (W_C).

(c). Shows the case where the sample is narrower than the beam. XFRAC is calculated as the ratio:-

(shaded area A_S) / (shaded area A_V).

Figure 1. The SANDALS diffractometer.

t_S

beam

3.2cm
beam

W_S

(a)

beam

t_{C1}

t_S

t_{C2}

W_C

(b) Top view

beam

A_V

3.2cm

Vanadium
slab

2.0cm

beam

A_S

3.2cm

Sample (flat plate
geometry)

(c)

Figure 2. Definition of dimensions used in input to ANALYSE
(Flat plate geometry).

(a). Shows the definition of sample thickness (t_S) and sample width (W_S).

(b). Shows the definition of cell thickness (t_{C1} and t_{C2}) and cell width (W_C).

(c). Shows the case where the sample is narrower than the beam. XFRAC is calculated as the ratio:- (shaded area A_S) / (shaded area A_V).
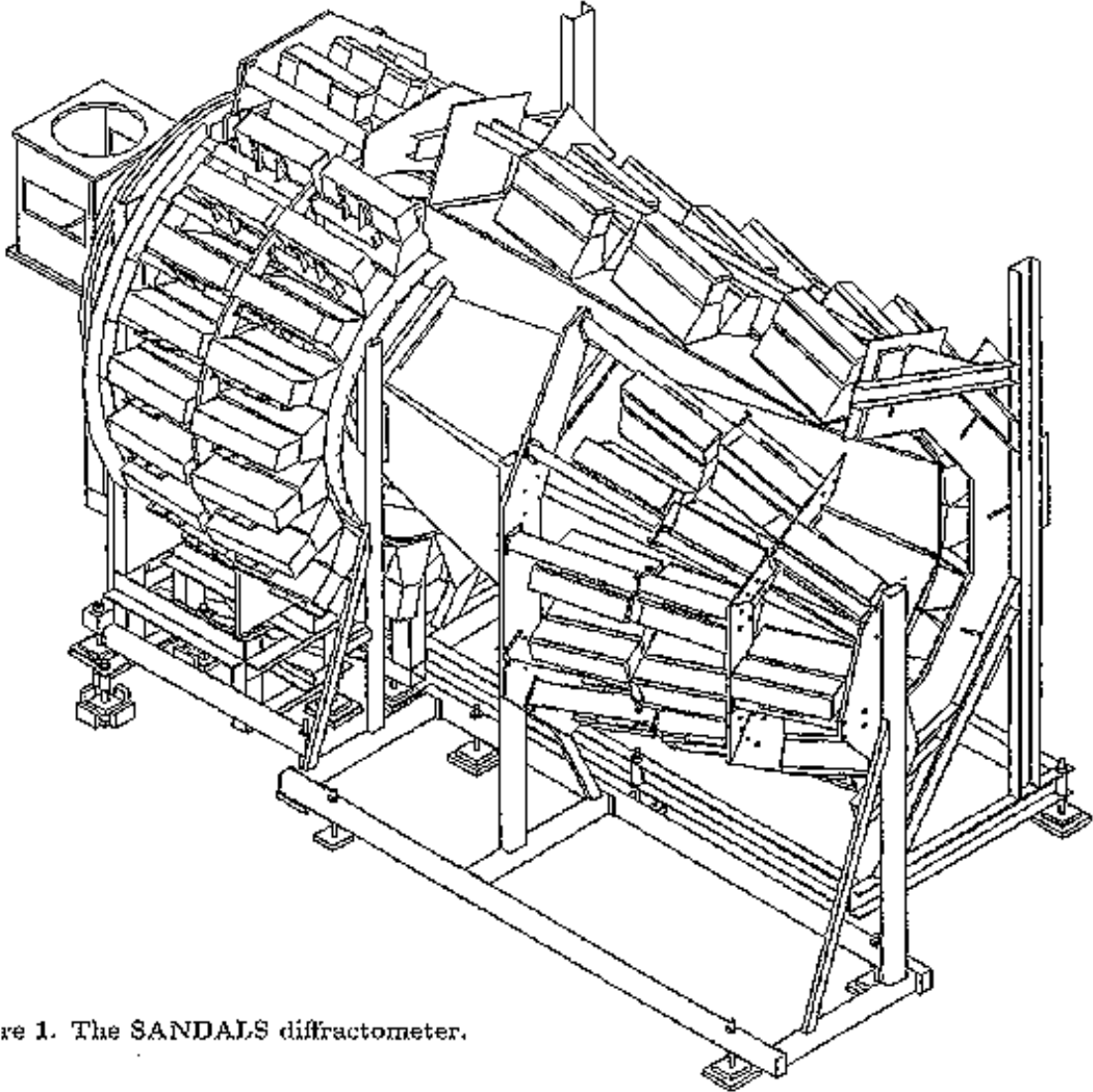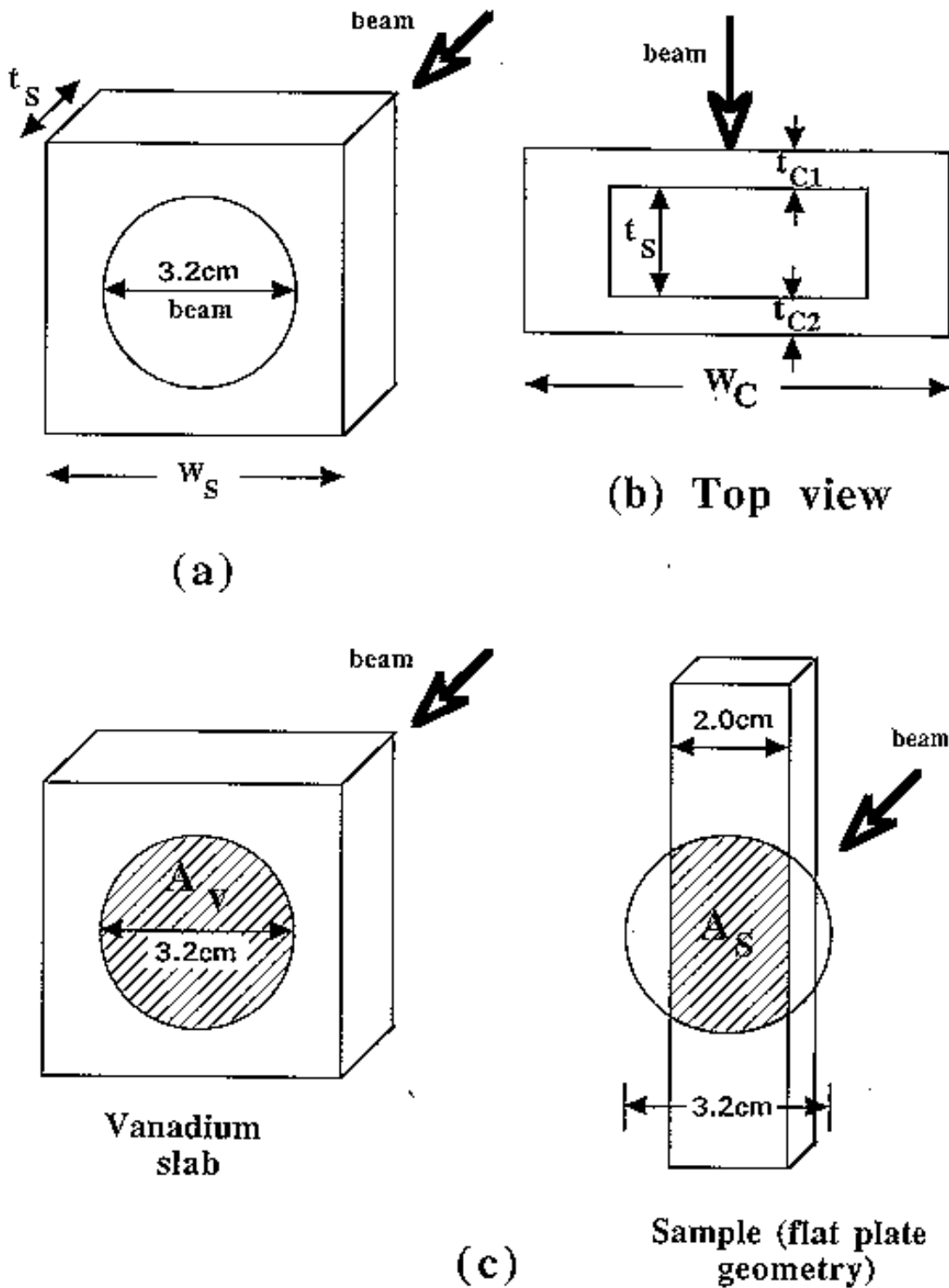
SECTION 5:

APPENDICES

Appendix A: Resolution of a time of flight diffractometer

The three dimensional quality of the transforms (1.2.1) or (1.2.2) has an important consequence when examining the effect of resolution broadening on peaks in S(Q).
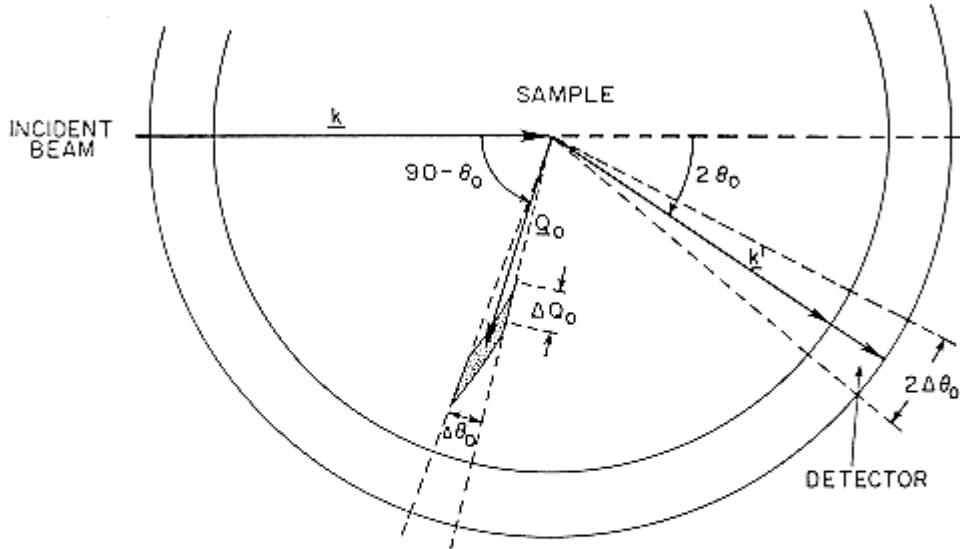

Figure A1 Geometry of scattering in reciprocal space

Figure A1 shows a projection of scattering space onto the $(Q, \theta, \phi=0)$ plane - in effect the Ewald sphere for the diffraction experiment. **k** and **k'** are the incident and scattered wave vectors, which are assumed to have the same magnitude, and the scattering angle is $2\theta_0$. With this geometry $|\mathbf{Q_0}| = 2k \sin \theta_0$. In fact two spheres, separated in Q by ΔQ_0, are shown corresponding to the edges of the time channel under consideration. The combination of angular uncertainty, pulse width and timing uncertainty means that at each time channel the detector probes a volume of reciprocal space (shown as the shaded area in Figure A1) whose magnitude is given approximately by

$$\Delta \mathbf{Q} = Q_0^2 \cos \theta_0 \, \Delta\theta_D \Delta\phi_D \Delta Q_0 = Q_0^2 \Delta\Omega \Delta Q_0 / 4\sin\theta_0 \qquad \text{A1}$$

provided ΔQ_0 and $\Delta\Omega$ are not too large. Here $2\Delta\theta_D$ and $\Delta\phi_D$ are the effective polar angular widths of the detector, and $\Delta\Omega = 2\sin2\theta_0\Delta\theta_D\Delta\phi_D$ is the solid angle of the detector. Note that since $\Delta\Omega$ is fixed for a given detector position, the volume of reciprocal space probed by the detector varies as $Q_0^2\Delta Q_0/\sin\theta$.

This volume of reciprocal space is not sampled uniformly by the detector. Instead we describe the distribution of $\mathbf{Q}$ vectors probed by the detector for a given scattering angle and time-of-flight channel by a RESOLUTION fucntion, $R(\mathbf{Q},\mathbf{Q_0})$, which incorporates all the effects which affect resolution e.g. pulse width, flight path uncertainty. For conservation reasons the resolution function must be normalizable:

$$\int d\mathbf{Q} \ R(\mathbf{Q},\mathbf{Q_0}) = 1 \qquad\qquad A2$$

Where the integral is taken in the volume around $\mathbf{Q_0}$. With this definition we can write down the measured structure factor (as opposed to that which would ideally be measured with infinitely sharp resolution) as

$$S_M(\mathbf{Q_0}) = \int d\mathbf{Q} \ S(\mathbf{Q}) \ R(\mathbf{Q},\mathbf{Q_0}) \qquad\qquad A3$$

The definition (A2) ensures that if, for example, $S(\mathbf{Q})$ is everywhere unity (e.g. a structureless fluid or purely incoherent scatterer) then $S_M(\mathbf{Q_0})$ is also everywhere unity as expected.

The consequence of this convolution on the measure pair correlation function can be seen if we insert (1.2.1) into (A3).

$$S_M(\mathbf{Q_0}) = 1 + \rho \int d\mathbf{Q} \ R(\mathbf{Q},\mathbf{Q_0}) \int d\mathbf{r} \ (g(\mathbf{r}) - 1) \exp(i\mathbf{Q.r})$$

$$= 1 + \rho \int d\mathbf{r} \ (g(\mathbf{r}) - 1) \ R(\mathbf{Q_0},\mathbf{r}) \qquad\qquad A4$$

where

$$R(\mathbf{Q_0},\mathbf{r}) \qquad = \int d\mathbf{Q} \ R(\mathbf{Q},\mathbf{Q_0}) \exp(i\mathbf{Q.r})$$

$$= \exp(i\mathbf{Q_0.r}) \int d\mathbf{Q} \ R(\mathbf{Q},\mathbf{Q_0}) \exp[i(\mathbf{Q-Q_0}).\mathbf{r}] \qquad\qquad A5$$

The simple Fourier transform in (1.2.1) is now replaced by a more complicated function which in general will not have a direct inversion. However if the Fourier transform of the resolution function (A5) can be calculated then the problem is amenable to forward transform techniques such as maximum entropy methods with no loss in computing time because the inherent linearity of the transform in preserved.

The resolution function is frequently estimated by convoluting the various contributions to the resolution function together. Such a convolution stricrly assumes the contributions are orthogonal which is only partly correct. However the convolution approach is valid in two limits, and probably gives satisfactory approximately results in intermediate cases as well. At small scattering angles, geometric effects dominate the resolution which usually means the effects of pulse width and flight path uncertainty can be ignored. On the other hand, at large scattering angles where geometric considerations assume less importance the resolution is dominated by the neutron pulse width, in which case the geometric effects can be represented by convolution of the pulse shape with a simple peak shape, usually Gaussian. The three main causes of resolution broadening will now be described briefly (see "Pulsed Neutron Scattering" by Colin Windsor [1]). These are the intrinsic pulse width for a given neutron energy or wavelength, Δt, the flight path uncertainty to the detector, ΔL, and the scattering angle uncertainty due to the finite size of the moderator, sample and detector.

A1.1 The neutron pulse shape

The pulse width is determined by moderator characteristics and so is independent of flight path and scattering angle and so is certainly orthogonal to the other contributions to the resolution function. It leeds to and uncertainty in the neutron's incident velocity, v, or wave vector , k, for a given time channel. The wave vector uncertainty in turn contributes to the uncertainty in the magnitude of **Q**, but not to the direction.

The neutron pulse shape at the moderator as a function of time t and neutron velocity v_0, is given by

$$P(t,v_0) = (\Sigma_s \, v_0 \, t)^2 \exp (-\Sigma_s \, v_0 \, t) \qquad\qquad A6$$

In the epithermal region, and this must be convoluted with a longer exponential tail in the thermal region [see Colin Windsor's book or notes from Andrew Taylor, RAL-84-120 (1984)]. For full details see the paper by Ikeda and Carpenter, Nucl. Inst. Meth. **A235**, 553 (1985). Σ_s is the macroscopic cross section of the moderating material. Note that the pulse shape is the same irrespective of whether it is presented as a function of t or v_0. When it reaches the detector after a flight path length L, the pulse shape is unchanged, but it is shifted in time by $t_0 = L/v_0$. Hence the pulse shape as a function of time at the detector is

$$P(t,t_0,v_0) = [\Sigma_s \, v_0 \, (t-t_0)]^2 \exp [-\Sigma_s \, v_0 \, (t-t_0)] \qquad\qquad A7$$

The pulse width correction arises in practice because we fix the time for a particular channel and evaluate the contribution of all reciprocal lattice points to that time channel by virtue of the velocity uncertainty of the neutron. In that case v_0 is the smallest neutron velocity that can reach the detector at time $t=t_0$. Hence the distribution of neutron velocities v (always greater than v_0) for this time channel is given by

$$P(t_0,v,v_0) = [\Sigma_s \, t_0 \, (v-v_0)]^2 \exp [-\Sigma_s \, t_0 \, (v-v_0)] \qquad\qquad A8$$

For liquids and amorphous diffraction there is the additional complication arising from the inelastic scattering of the sample. However, since the interference inelasticity correction tends to be small in many cases, it is unlikely that inelasticity will have a very pronounced effect on the observed resolution. Thus for the present purpose it will be assumed that the scattering is elastic.

We write $\hbar k = mv$, where k is the neutron wave vector and m the neutron mass, and with $k_0 = mL/\hbar t_0$, $Q=2k \sin\theta$ and $Q_0 = 2k_0 \sin\theta$, the pulse shape in reciprocal space appears as

$$P(Q, Q_0) = [\Sigma_s \, L(Q-Q_0)/Q_0]^2 \exp [-\Sigma_s \, L \, (Q-Q_0)/Q_0] \qquad\qquad A9$$

In this form the advantage of going to a longer flight path can be seen explicitly - as L is made larger the pulse decays more rapidly and becomes narrower in reciprocal space. Also it will be seen that the FWHM of the resolution function $\Delta Q/Q = \Delta\lambda/\lambda$ = constant for a given total flight path.

A1.2 Flight path uncertainty

The flight path uncertainty arises because we necessarily must use finite size moderators, samples and detectors. Therefore it depends closely on the particular instrumental geometry. Furthermore it cannot be regarded as decoupled from the scattering angle uncertainty since different points in the moderator, sample and detector may define different scattering angles as well as different flight paths. Therefore the normal approach is to treat flight path uncertainty as part of the geometric contribution to the resolution of a diffractometer. It is incorporated into the scattering uncertainty as an "effective" angular uncertainty.

A1.3 Scattering angle uncertainty

The scattering angle uncertainty of recorded events in the detector lead to an uncertainty in $\mathbf{Q}$, $\Delta\mathbf{Q}$, both in direction and magnitude, in a manner which varies depending on the precise details of the instrument geometry. Normally for accurate numbers, the geometric contribution to the resolution function has to be determined by computer simulation of a model of the instrument, or by measuring the profile of Bragg peaks. Since the results of such a simulation indicate that the geometric contribution is usually quite symmetric, except at very small scattering angles, it is useful to represent the angular uncertainty with an effective angular width for the detector , $2\Delta\theta_D$. In fact, the geometric contribution is usually found to be roughly Gaussian in $\Delta\theta$, where $2\Delta\theta$ is the difference between the nominal scattering angle of the detector, $2\theta_0$, and the actual scattering angle 2θ, of a particular neutron event in the detector. Provided $\cot\theta\Delta\theta_D$ is ~10% or less and $\Delta\theta$ has a symmetric distribution about θ_0 , then the geometric contribution to the resolution is roughly symmetric irrespective of whether it is presented as a function of wavelength, time or Q.

For the geometric contribution a reasonable approach is to assume that the scattering angles probed by the detector are distributed in a Gaussian manner about $\theta=\theta_0$. This assumption can be verified to be approximately correct for the typical instrumental geometries which occur in practice. In that case we describe the distribution by

$$P(\theta,\theta_0) = \exp\left[-(\theta-\theta_0)^2/2\gamma^2\right] = \exp\left[-\Delta\theta^2 / 2\gamma^2\right] \qquad\qquad \text{A10}$$

Where γ describes the angular width of the distribution and it is assumed that $\gamma<<\theta_0$. Writing $\Delta Q = 2k\cos\theta_0\Delta\theta = Q_0 \cot\theta_0 \Delta\theta$ we see that the geometric contribution to the resolution function in reciprocal space is represented by

$$R_G(Q,Q_0) \sim \exp\left[\Delta Q^2/2Q_0^2\gamma_Q^2\right] = \exp\left[-(Q-Q_0)^2 / 2Q_0^2 \gamma^2\right] \qquad\qquad \text{A11}$$

Where $\gamma_Q = \gamma \cot\theta_0$. The normalisation condition (A2) with (A1) then requires that

$$R_G(Q,Q_0) = A \exp\left[-(Q-Q_0)^2 / 2Q_0^2 \gamma^2\right]$$

Where

$$A = 1 / \sqrt{(2\pi)} Q_0^2 \sin\theta_0 \Delta Q_0 \Delta\phi_D \gamma_Q$$

In solving the integral (A2) for this function we note that the integral over ϕ coordinate of the detector does not affect the magnitude of Q, and we have assumed that the incident wave vectors are distributed uniformly over ΔQ_0. This form exhibits the well known result that the width of the geomtric contribution, $\Delta Q/Q$, to the resolution function is constant for a given scattering angle, and varies with scattering angle θ_0 as cot θ_0.

A1.4 Application to liquids and amorphous materials diffraction

For an instrument such as SANDALS the geometric term dominates the resolution function for scattering angles below about 40°. Since this is the important measuring region, as far as minimizing Placzek corrections is concerned, we can safely assume that an expression such as (A12) will adequately represent the resolution of the diffractometer. With this choice the Fourier transform of the resolution function (A5) can be evaluated analytically. First we note that for this case (and also polycrystalline materials) the integrals over the directions of **Q** in (A3) can be done immediately to give

$$S_M(Q_0) = (1/\sqrt{(2\pi)}Q_0\gamma_Q) \int_0^\infty dQ \exp [-(Q-Q_0)^2/ 2Q_0^2\gamma_Q^2] \, S(Q) \quad A13$$

Inserting the definition for S(Q) (1.2.2) into (A13) leads to the result:

$$S_M(Q_0) = 1 + 4\pi\rho \int_0^\infty dr \, r^2 \, (g(r)-1) \, R(Q_0,r) \qquad A14$$

where

$$R(Q_0,r) = (1/\sqrt{(2\pi)}Q_0\gamma_Q) \int_0^\infty dQ \exp [-(Q-Q_0)^2/ 2Q_0^2\gamma_Q^2] \sin(Qr)/Qr$$

Writing $Q=Q_0 + Q'$ and assuming that always $|Q'|<<Q_0$, this last integral can be solved analytically using standard integral tables (see Gradshteyn and Ryzhik, p 480 and p 495, 1980 edition, Academic press, London). To second order in γ_Q the result is

$$R(Q_0,r) = [\sin(Q_0r)/Q_0r - \gamma_Q^2 \cos(Q_0r)] \exp [-r^2Q_0^2\gamma_Q^2/2] \qquad A15$$

Therefore the main effect is that the exact transform of equation (1.2.2) is modulated by a Gaussian decay caused by the finite resolution in Q space.

Appendix B: Estimating the count rate on a TOF diffractometer

As the features in a liquid or amorphous material's diffraction pattern are rather broad (compares to crystallin powder diffraction) the requirements for resolution are relatively relaxed (provided very large Q values are not needed), but an adequate count rate can be crucial to obtaining a useful result. This is particularly the case for those experiments which involve differencing data sets as a function of pressure, temperature, isotope etc. In these cases the differential behaviour is usually more important than the total scattering pattern. Therefore count rate is almost always the primary quantity of interest. Typically the data are mapped out as a function of Q in bins of width $\Delta Q = 0.05 \text{Å}^{-1}$, and the quantity of interest in rating the performance of a diffractometer is therefore the count rate per Q-bin per unit volume of standard scatterer which is normally vanadium:

Neutrons / s / 0.05Å^{-1} / cm^3 of vanadium B1

This definition serves to normalize out differences between instruments which are purely geometric in origin, (usually the size and shape of the beam at the sample position.)

This number is also useful to know for a given diffractometer: a rough estimate of the count rate for a given sample can be obtained by multiplying it by the volume of the sample times the ratio of the sample scattering cross section to vanadium scattering cross section. It would be helpful therefore if this number could be specifies for all liquids diffractometers so that realistic intercomparisons could be made. For convenience we shall refer to the count rate number according to (B1) as the "C-number" for a given diffractometer.

For reactor experiments the count rate is almost independent of Q, but for pulsed sources the spectrum falls as $1/Q$ in the epithermal region. In addition the detector efficiency is proportional to $\lambda \sim 1/Q$, so the measured count rate falls as $1/Q^2$. In practice, efficiency corrections mean that the intensity falls more like $1/Q^{1.7}$, but even so there is a dramatic fall in measured count rate with increasing Q.

For the methane moderator at ISIS the parameter that describes the epithermal flux is Φ_0 and at 100μA proton current and 750MeV energy, this has the value for a moderator area of $100cm^2$ (see Table 1.1)

$$\Phi_0 = 2.7 \times 10^{12} / E^{0.92} \text{n/ev/sr/}100cm^2\text{/s}$$

Now $E \sim Q^2$ so $\Phi(Q) = 2(E/Q)\Phi(E)$

$$\cong 5.4 \times 10^{12} / Q \text{ n/Å}^{-1}\text{/sr/}100cm^2\text{/s}$$

$$= 2.7 \times 10^{11} / Q \text{ n/}0.05\text{Å}^{-1}\text{/sr/}100cm^2\text{/s}$$

Using these values the expected count rate on SANDALS can be estimated. It is assumed that:

(1) The collimator views most of the active area of the moderator
(2) The incident flight path is **11** metres.
(3) The sample is a cube of vanadium, 10x10x10mm³ in volume (corresponding to a 30% scatterer)

(4) Each ZnS element in the detector is **10**% efficient at $\lambda=1$Å, and there are 20 elements making up each detector. This gives an efficiency of 87% at 1Å and 35% efficiency at 0.2 Å. ($I_t = 0.9 = I_0 \exp[-\Delta]$ so for 20 elements and $\lambda=0.2$Å, $E(\lambda)=1-\exp[-20\Delta\lambda] = 0.35$)

Then the scattered count rate per unit detector solid angle is

2.7×10^{11} x   0.3   x 8×10^{-7} x $0.35 / 4\pi Q$

moderator   fraction scattered   sample solid   detector efficiency
           by sample   angle at moderator

$= 1804/Q$ n/0.05Å^{-1}/sr/s/cm^{3}V.   B4

It will be noted that this number, which of course applies strictly only to the epithermal region of the spectrum, is independent of scattering angle for a given Q value. The fact that count rates vary for different scattering angles in practice arises primarily from variations in detector solid angle and efficiency. For SANDALS at $2\theta=20°$ (Group 1) the detector area is 60 detector elements $* 0.01 * 0.2$ m^2 and the final flight path is 2.51m, and so for $Q=10$Å^{-1}, the C number is 3.4 n/0.05Å^{-1}/s/cm^{3}V. The C number is quoted at 10Å^{-1} since it is important to remember the very rapid decline in count rate at a pulsed diffractometer with increasing Q value. Bearing in mind that the SANDALS instrument has 1270 detectors in 18 banks, the C-number rapidly becomes much larger.

Finally, for the D4B diffractometer at ILL, the measured neutron flux on the sample is 4×10^7 n/cm^2/s for a wavelength of 0.7Å, so the C-number for the standard cube of vanadium would be

4×10^7 x   0.3   x 5.5×10^{-4} x   0.67   x $0.15 / 4\pi$

flux   fraction scattered   detector solid   detector   sampling factor
      by sample   angle for 0.05Å^{-1} efficiency
                   bins

     $= 53$ n/0.05Å^{-1}/s/cm^{3}V

The sampling factor arises here because the present detector does not scan all scattering angles simultaneously. This number is entirely in accord with the observed count rate from a sample of vanadium placed in the neutron beam on D4B (A.C.Barnes, 1988 private communication.)

The measured SANDALS C-number November 2000
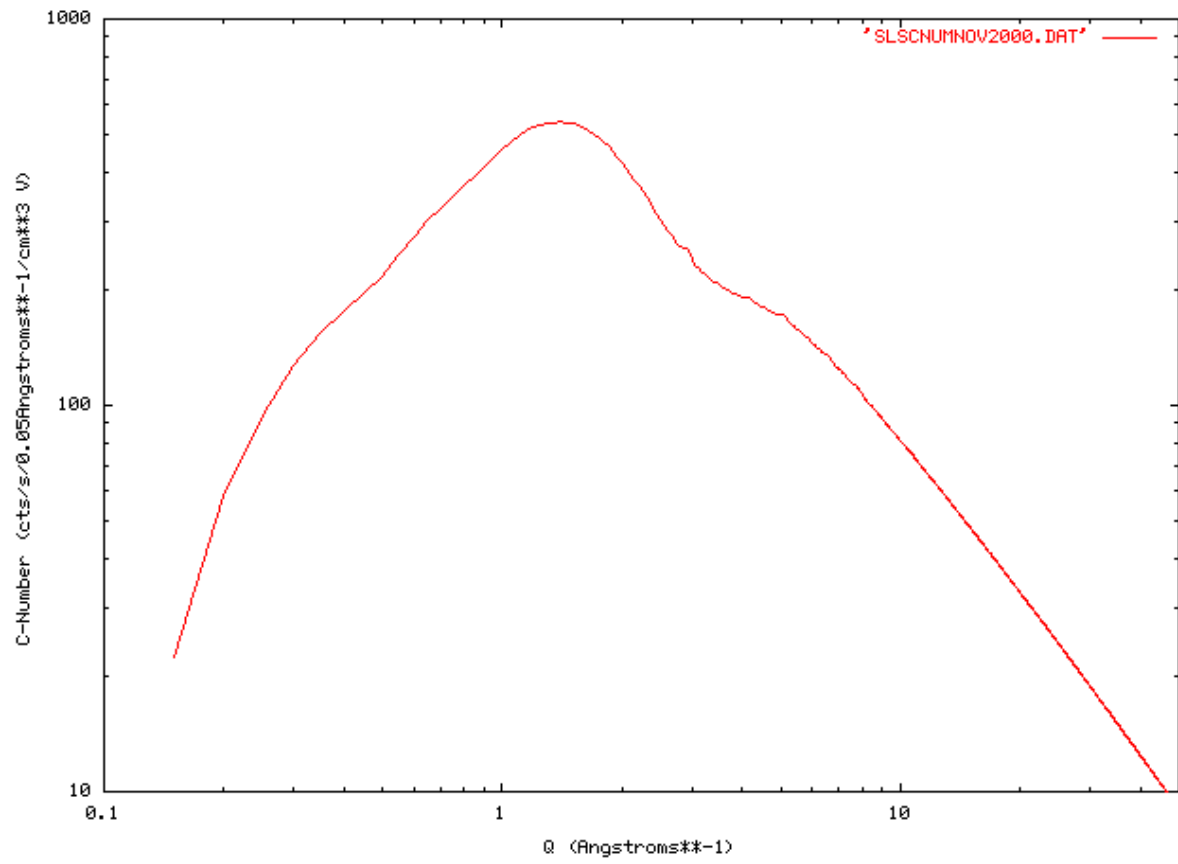
Appendix C: Maximum entropy methods in neutron scattering - application to the structure factor problem in disordered materials

C.1 Introduction

A broad class of problems in neutron scattering involve the inversion of a set of measurements, the data D_I, to a desired distribution function, N_j, the N_j being related to the D_I via a transform of some kind:

$$D_I = Tr \{ N_j \} \qquad i,j = 0,1,.....,\infty \qquad (C1)$$

This inversion is often impossible of ill-conditioned for several reasons:

    (a) The transform may not be linear;
    (b) The data may be incomplete, $i = i_1 \ldots i_2$;
    (c) The data are measured at discrete points;
    (d) The data may be noisy;
    (e) The data may have systematic errors.

Due to this ill-conditioning, it is likely that several or perhaps a large set of distributions N_j can be regarded as consistent with the measured data.

Over the years a large number of methods have evolved to cope with the variety of difficulties which arise in the inversion of incomplete data. Of these, it is claimed, Jaynes [22], that the maximum entropy (ME) approach, which attempts to avoid producing any information which is not justified by the data, provides an independent assessment of all the possible solutions to a particular problem, and so leads to that solution which is "maximally non-committal" with respect to the unmeasured data. This is achieved via an entropy metric which is usually defined as:

$$H = -\sum_j N_j \ln \{N_j/P_j\} + \sum_j N_j - \sum_j P_j \qquad (C2)$$

Where P represents a "prior" distribution which incorporates previous knowledge about the distribution not contained in the data. The second and third terms are introduced in (C2) in the event that N and P are not normalizable distributions. In the absence of any other information the ME solution, which attempts to maximize H, is simply N=P for all j. When constrained by additional information, i.e. the measured data, the entropy falls below its maximum value. The object of the ME method there is to find that solution for N which satisfies the data but which also keeps H as near as possible to its maximum value. It will be seen that this definition of H only exists if $N_j, P_j > 0$.

The goodness of fit to the data is usually measured by a χ^2 statistic or R-factor:

$$R_f^2 = \sum_i (D_i - M_i)^2 / \sum_i D_i^2 \qquad (C3)$$

Where M_i
Is an estimate (or "model") of the i'th data point obtained from the estimated trial N distribution via (1). With this definition a "quality factor", or Q-factor, which represents how

well a particular solution satisfies the dual constraints of entropy maximisation and fit to the supplied data, is defined as

$$Q_f^2 = -H + xR_f^2 \qquad\qquad (C4)$$

Where x is an undetermined positive multiplier which controls how closely the model fits the data. Therefore it is the Q-factor which is to be minimized, with x determined by constraining the R-factor to a predefined value.

In setting up the ME solution for a given experimental situation, there are two questions that need to be confronted. Firstly what is the most appropriate distribution space, the N distribution, in which entropy is to be calculated? Secondly, what is the most reasonable choice for the prior distribution, or P distribution. It is frequently assumed that the prior distribution should be uniform even though the existence of the data implies that the real distribution is anything but uniform. Unfortunately both of these questions are often ignored in the literature, there being an implicit assumption that somehow maximizing the entropy will cover up all of the difficulties. In the sections that follow, I will apply the ME method to the problem of calculating the pair correlation function for a liquid or amorphous material from structure factor data. I will demonstrate that the obvious choice for the distribution N is in fact quite inappropriate in this case, and that the result of the ME analysis can depend markedly on the choice of prior distribution. Full details on the correct choice for the N and P distributions for the entropy estimation for this problem are given elsewhere, but some examples of the results are shown here. The conclusions to be drawn are applicable ot many other applications where ME techniques are used.

C.2 Solution of the maximum entropy problem

The general solution of the ME problem is a highly non-linear problem and several solutions exist, mostly using sophisticated search procedures, Bryan and Skilling [23]. I have developed a Monte Carlo (MC) solution to this problem which has several attractive features. In particular it is simple to execute, can allow error bars on the calculated distributions to be estimated if needed, and by virtue of the stochastic process intrinsic to MC calculations is unlikely to get stuck in local phase space minima. The object of the MC calculation is to set up an ensemble of distributions such that each member occurs with probability

$$p(Q_f^2) = \exp\{ -\lambda Q_f^2 \} \qquad\qquad (C5)$$

with λ a positive multiplier which determines the size of the Q factor and its fluctuations: as λ is made larger, so the Q-factor is driven smaller and the fluctuations become smaller. Full details of this algorithm are given elsewhere, and will not be elaborated further here. However it will be noted that in all the examples given below, λ is kept as large as possible, so that fluctuations are held to a minimum and the individual trial distributions lie indistinguishably close to the ME solution. Typical runs of this algorithm might involve 500,000 individual moves, 200 data points and 500 points in the N distribution.

C3 The structure problem in disordered systems

The underlying transform in the structure of liquids and amorphous materials is in principle a straightforward Fourier transform:

$$S(Q) = 4\pi\rho \int_0^\infty r\,\{g(r)-1\}\,\sin(Qr)\,dr \qquad\qquad (C6)$$

where $S(Q)$ is the measured structure factor, as a function of wave vector transfer, Q, and $g(r)$ is the underlying pair distribution function as a function of radial distance r from an atom at the origin. The atomic number density is ρ. Inverting this transform directly can lead to significant transform error, statistical or systematic. Typically one introduces the constraint of only calculating $g(r)$ at certain values of r, according to the Lado [24] rules for Fourier transforms, i.e. $\Delta r = \pi/Q_{max}$. Furthermore a "window" function is often invoked to further reduce the effects of noise in the calculated distribution function.

This problem is readily amenable to ME analysis. In particular there is apparently an obvious choice for the N distribution by virtue of the normalization

$$4\pi\rho \int_0^\infty r^2\,\{g(r)-1\}\,\sin(Qr)\,dr = -1 + \rho\chi k_B T \qquad\qquad (C7)$$

where χ is the isothermal compressibility and T is the absolute temperature. Hence the "obvious" choice for the N distribution is simply

$$N_j = N(r_j) = 4\pi\rho r_j^2 g(r_j)\Delta r \qquad\qquad (C8)$$

Where Δr is the bin width of the discretized distribution function. Figures C1 and C2 show the effects of applying ME analysis to the problem of transforming the hard sphere structure factor to pair correlation function.

In this case the input $S(Q)$ is known exactly within the Percus-Yevick approximation but is a particularly severe test of any transform method because $g(r)$ for hard spheres is discontinuous at $r=\sigma$, the hard core diameter. In this case the density was chosen such that $\rho\sigma^3=0.5$ and a large Q limit of $Q_{max}=15/\sigma$ was imposed on the $S(Q)$ data, with $\sigma=1$Å. In figure C1 the prior distribution is

$$P_j = 0 \qquad\qquad \text{for } r_j < \sigma$$
$$\qquad\qquad\qquad\qquad\qquad\qquad\qquad (C9)$$
$$P_j = 4\pi\rho r_j^2\Delta r \qquad\qquad \text{for } r_j > \sigma$$

While for figure C2 the prior distribution is set at

$$P_j = 0 \qquad\qquad \text{for } r_j < 0.75\sigma$$
$$\qquad\qquad\qquad\qquad\qquad\qquad\qquad (C10)$$
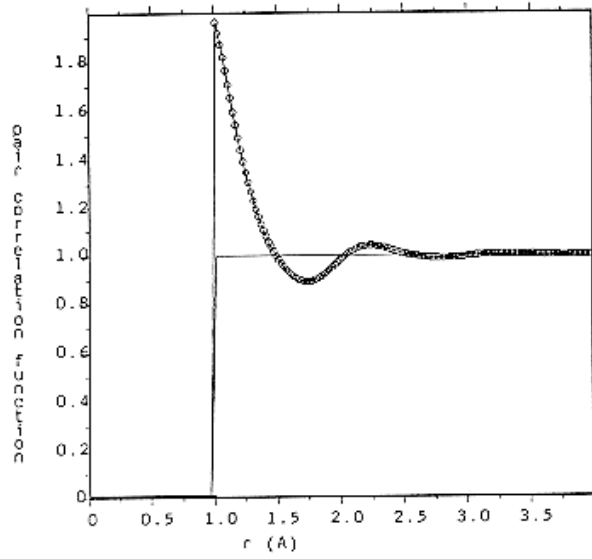$$P_j = 4\pi\rho r_j^2\Delta r \qquad\qquad \text{for } r_j > 0.75\sigma$$

Figure C1 Maximum entropy pair correlation function derived from Percus
Yevick hard sphere structure factor. The $S(Q)$ data were truncated at Q
$= 15\text{\AA}^{-1}$, and the prior distribution used is zero in the region $r = 0$ to
$r = 1\text{\AA}$. The circles show the calculated distribution and the line shows
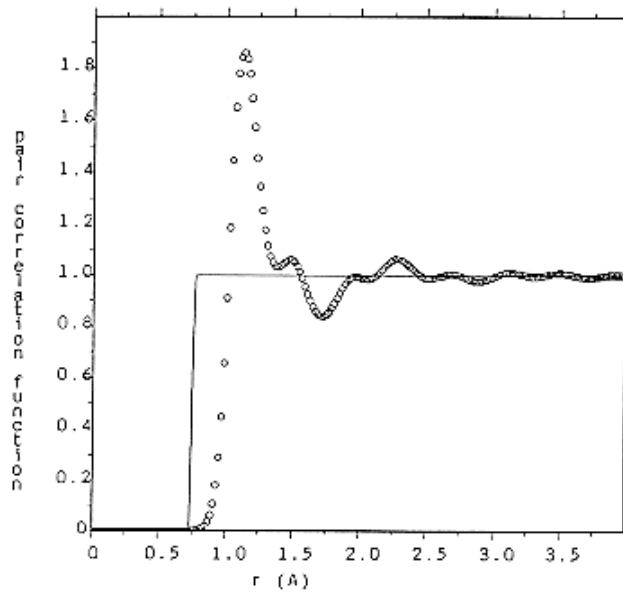the prior.

Figure C2 Same calculation and notation as for figure 1 except that the
prior is zero in the region $r = 0$ to $r = 0.75\text{\AA}$.

101

In either case the fit to the data was the same, (R-factor = 1%); however it is readily apparent that the two results for g(r) are not the same. In particular the distribution in figure C2 has greater entropy than figure C1 (-2.064 for figure C2 compared to –2.534 for figure C1) when measured against the uniform prior, thus confirming that the algorithm has found the true maximum entropy solution for figure C2. This result is apparently at odds with our intuition which might tend to favour the one in figure C1 as being less "structured", if the word "structure" in this case is taken to indicate the number and size of peaks and valleys in the calculated distribution. In fact the distribution in figure C1 is very close to the known exact solution, Throop and Bearman [25].
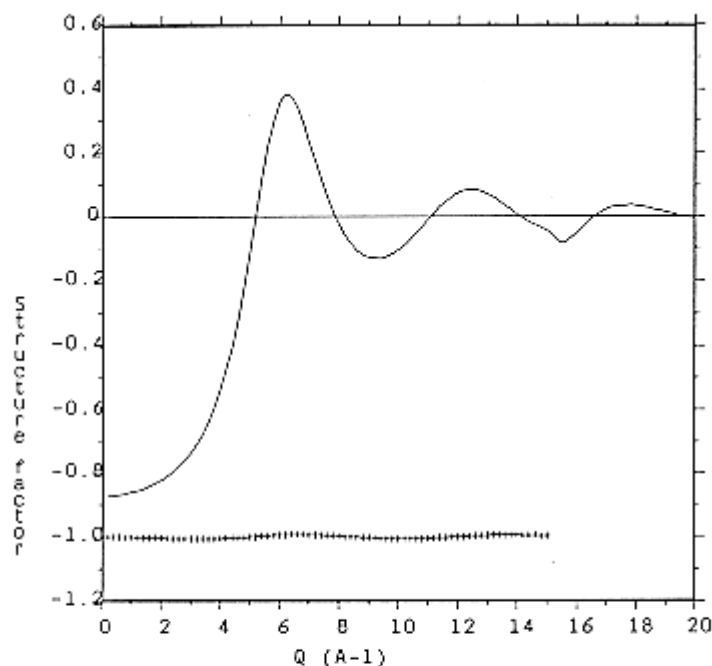

Figure C3 Maximum entropy structure factor corresponding to the correlation function of figure C2. The crosses show the residual between fit and data shifted below zero by unity.

The difference between the two solutions is manifested in Q-space not in the region of the input data, where the two solutions give equally good fits, but beyond the input region. Figure C3 shows the calculated structure factor for the distribution in figure C2, and also the difference between the model and data. It is seen that immediately beyond the data (Q ~ 15-16Å^{-1}) there is a strange cusp in the S(Q) from figure C2, a phenomenon which has been seen before, Root, Egelstaff and Nickel [26]. The ripples seen in figure C2 become suspect when it is realized they have a period of $2\pi/Q_{max}$, where Q_{max} is the largest Q-value for the input data. Hence it is concluded that maximizing the entropy has not avoided the truncation ripples associated with the discontinuity in the input data at $Q=Q_{max}$. For measured datasets which usually have a noise component, the discontinuities become important since there is effectively a discontinuity at every data point.

C.4 Solution of the discontinuity problem

Two solutions to the problem of discontinuities are proposed. The first is to effectively force $S(Q)$ to be everywhere continuous and have continuous derivatives. To see show to do this a well known theorem from Fourier transforms is invoked, Lighthill [27]. From (C6) it can be seen that the n'th derivative of $S(Q)$ is given by:

$$S^n(Q) = 4\pi\rho(-1)^{n/2} \int_0^\infty r^{n+1} \{g(r)-1\} \sin(Qr)\, dr \qquad \text{for n even} \qquad (C11)$$

and

$$S^n(Q) = 4\pi\rho(-1)^{(n-1)/2} \int_0^\infty r^{n+1} \{g(r)-1\} \cos(Qr)\, dr \qquad \text{for n odd} \qquad (C12)$$

Therefore if $\{g(r)-1\}$ converges slower than $1/r^{n+2}$ as $r\to\infty$, there will be discontinuities in the n'th derivative. On the other hand if $\exp(\alpha r)\{g(r)-1\}$, where α is a finite positive number, is convergent as $r\to\infty$ the $r^{n+2}\{g(r)-1\}$ is also convergent at large r for all n. For the hard sphere pair correlation function the exponential decay of $\{g(r)-1\}$ with increasing r is an analytic consequence of the theory which describes the hard sphere structure factor, Perry and Throop [28]. For other liquid and amorphous structures the requirement that $S(Q)$ be continuous and have continuous derivatives is a necessary consequence of there being no long range order in the material.

This exponential constraint leads to a simple revision of the definition of the N and P distributions, namely:

$$N_j' = \exp(\alpha r_j) \times N(r_j) = 4\pi\rho \exp(\alpha r_j) r_j^2 g(r_j)\Delta r \qquad (C13)$$

And

$$P_j' = 0 \qquad\qquad \text{for } r_j < \sigma$$

$$P_j' = 4\pi\rho \exp(\alpha r_j) r_j^2 g(r_j)\Delta r \qquad \text{for } r_j > \sigma$$

$(C14)$

The primed distributions are used instead of the unprimed distributions in the definition of entropy, equation C2. Otherwise the calculation proceeds as before. The inverse correlation length, α, is determined from the width of the narrowest peak in $S(Q)$, or by inspection of the large r behaviour of $g(r)$. Hence for a previously unknown dataset, it may be necessary to redetermine its value once an initial solution has been achieved.

Figures C4 and C5 show the results of applying this exponential constraint in the definition of entropy, with $\alpha = 1.8/\text{Å}$. It can be seen that the repples in figure C2 have been largely eliminated in the figure C4 and that the problem of the cusp in $S(Q)$ and $Q=Q_{max}$ has now been erradicated (figure C5). The fit is as good as before (R-factor =1%) and the entropy is only marginally lower than for figure C2, being equal to -2.096.
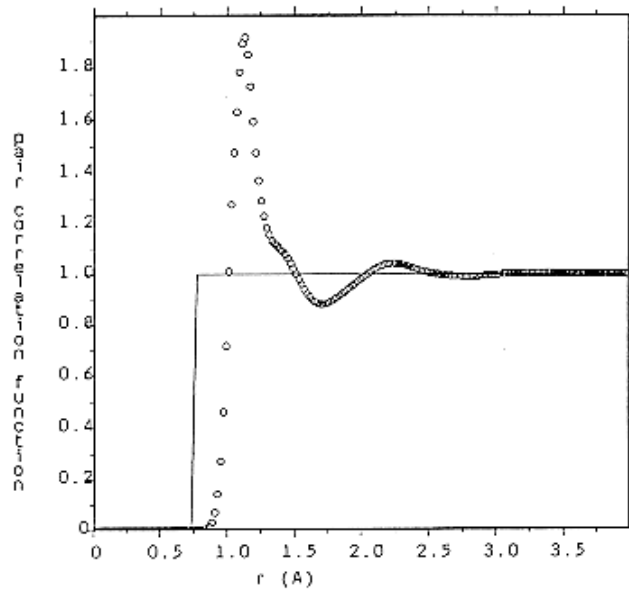
Figure C4 Maximum entropy pair correlation function as for figure 2, but this time derived using the exponential weighting on the distributions used to calculate the entropy, as described in the text.
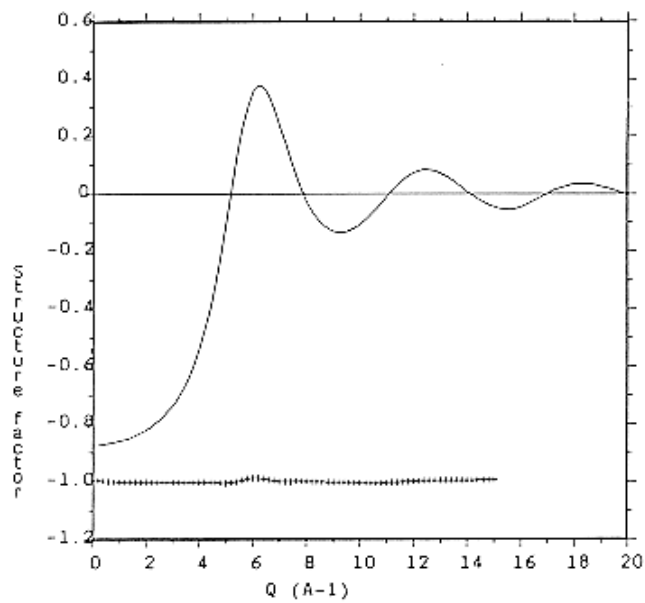

Figure C5 Maximum entropy structure factor corresponding to figure 4. Note that the cusp near Q = 15/Å is absent in this case.

C.5 Coping with truncation effects

It is apparent in figure C4 that some truncation effects may still be present in the estimated distribution functions. These arise because in estimating the change in Q-factor at each move, there is a sum over the input data which in effect is a Fourier transform of the difference $D_i - M_i$. Since the change in Q factor at each move is the driving force behind the calculation, this Fourier transform can give rise to exactly the same truncation effects seen in a direct transform of the raw data. My solution to this difficulty is to evaluate the transform only at the allowed r values ($r_j = j\pi/Q_{max}$), and then interpolate the result onto the required grid of r values by linear interpolation.

Figure C6 shows the result of doing this for the same input dataset as before. Now it will be noted that truncation effects are diminished even further: the result is now approaching that of Figure C1, but with greater entropy (H=-2.141).
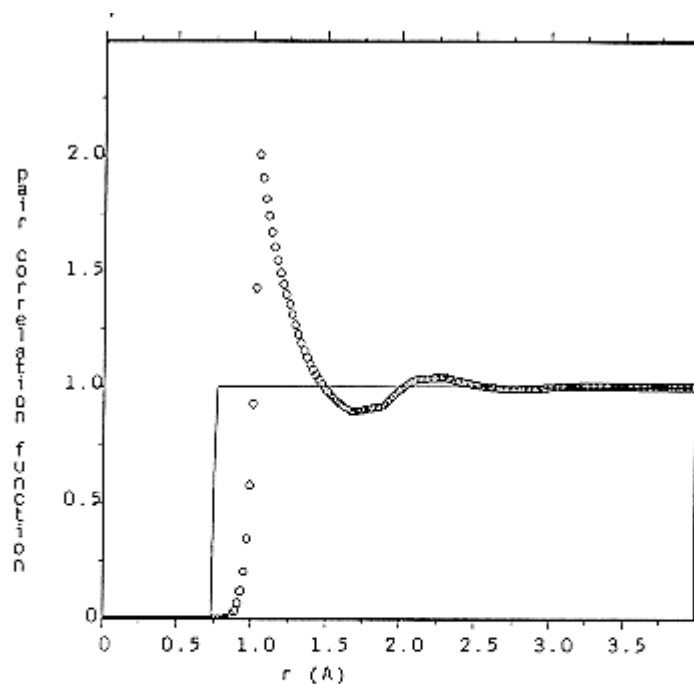
Figure C6 Maximum entropy pair correlation function as before, but this time using the fluctuations in the Q-factor linearly interpolated between the allowed discrete Fourier values.

C.6 Conclusion

The foregoing text has described the application of the ME method to the calculation of the pair correlation function from structure factor data for liquid and amorphous materials. The main conclusion is that ME does not automatically gurantee that the results are free from artifacts associated with noise and truncation in the data. To avoid these artifacts it is necessary to build into the distributions used to calculate entropy, known physical constraints which must be satisfied, whatever the detailed form the distributions are to take. For the

structure factor problem these constraints include the requirement that the structure factor must everywhere be continuous and have continuous derivatives, and that the fluctuations in the distributions away from the prior distribution are not biased by the truncation of the input data. Further details and applications of the Monte Carlo algorithm used here are available elsewhere as well as a discussion of the present approach in the context of other recent attempts at the structure factor problem.

C.7 Acknowledgement

APPENDIX D: NEUTRON ABSORPTION RESONANCES

Z	Element	Resonance energies (eV)				
17	^{35}Cl	400				
23	V	170				
25	Mn	350				
27	Co	140				
29	^{63}Cu	600				
	^{65}Cu	240				
30	^{67}Zn	220	450			
	^{68}Zn	510				
31	^{69}Ga	110	350			
	^{71}Ga	95	300			
32	Ge	100	110	200		
33	As	46	95	250		
34	Se	2.6	210	270		
35	Br	35	55			
36	Kr	28	41	110		
38	Sr	3.5	600			
40	Zr	300	700			
41	Nb	35	42	95		
42	Mo	12	45	70		
43	Tc	5.6	20	40		
44	Ru	10	15	25		
45	Rh	1.2	34	46		
46	Pd	3	13	25		
47	^{107}Ag	16	40			
	^{109}Ag	5	30	40		
48	Cd	0.18	19	29		
49	In	1.5	4	9	12	
50	Sn	40	45	65		
51	Sb	6	15	21		
52	Te	2.3	8.5	25		
53	I	20	31			
54	Xe	5	9.4	14		
55	Cs	6	22	50		
56	Ba	25	80			
57	La	7				
59	Pr	85	210			
60	Nd	4.3	45	55		
61	Pm	5.4	6.9	7.0	16	
62	^{147}Sm	3.4	18			
	^{149}Sm	0.1	0.9	5	9	15
	^{152}Sm	8				
63	Eu	0.5	1	2.5	3.4	
64	Gd	2.1	2.6	2.9	6.3	7
65	Tb	3.3	11			
66	Dy	1.7	2.7	3.7		
67	Ho	3.9	12.8			

68	Er	0.45	0.58	4.4	6	9
69	Tm	3.9	14	17.5		
70	Yb	0.6	7.9	13		
71	Lu	0.14	2.6	5.2		
72	Hf	1.1	2.4			
73	Ta	4.3	10.3	14		
74	W	4.2	7.6	18.8		
75	Re	2.16	4.4			
76	Os	6.7	9.0	10.3		
77	Ir	0.66	1.3	5.4		
78	Pt	12	20			
79	Au	4.9	60	80		
80	Hg	23	32			
81	Tl	240				
88	Ra	0.5				
90	Th	22	23	60		
91	Pa	0.4	5			
92	^{233}U	1.8	2.3	6.8		
	^{234}U	5.2				
	^{235}U	8.8	11.7	12.4	19.3	
	^{236}U	5.4				
	^{238}U	6.67	20.9			
93	Np	0.5	1.5			
94	^{238}Pu	2.9	10	18		
	^{239}Pu	0.3	7.8	11		
	^{240}Pu	1.06	20.5			
	^{241}Pu	0.3	4.3			
	^{242}Pu	2.7				
95	Am	0.3	0.6	1.3		

References

1. Windsor C, 1981 "Pulsed Neutron Scattering", Academic Press
2. Taylor A D, 1984 Rutherford Appleton Report RAL-84-120
3. van Hove L, 1954, Phys. Rev. **95,** 249
4. Egelstaff P A, 1987 "Neutron scattering", Ed. K Sköld and D L Price, ch 14, Academic Press series – Methods of experimental physics, vol 23, part B
5. Placzek G, 1952, Phys. Rev. **86,** 377
6. Powles J G, 1973, Mol. Phys. **26**, 1325
7. Rickayzen G and Powles J G, 1976, Mol. Phys. **32**, 301
8. Powles J G and Rickayzen G, 1976, Mol. Phys. **32**, 323
9. Powles J G, 1978, Mol. Phys. **36**, 1161
10. Powles J G, 1978, Mol. Phys. **36**, 1181
11. Powles J G, 1979, Mol. Phys. **37**, 623
12. Egelstaff P A and Soper A K, 1980, Mol. Phys. **40** 553
13. Egelstaff P A and Soper A K, 1980, Mol. Phys. **40** 569
14. Koester L, Rauch H, Herkens M, Schröder, 1981 "Summary of Neutron Scattering Lengths", KFA-Jülich report no. 1755
15. Sears V F, 1984, "Thermal neutron scattering lengths and cross sections for condensed matter research", Atomic Energy of Canada Limited, Chalk River, Ontario, Canada, AECL report No. 8490
16. Soper A K and Egelstaff P A, 1980, Nucl. Inst. Meth., **17**
17. Paalman H H and Pings C J, 1962, J. Appl. Phys. **33**, 2635
18. Blech I A and Averbach B L, 1965, Phys. Rev. **137A**, A1113
19. Sears V F, 1975, Adv. Phys. **24**, 1
20. Howe M A, McGreevy R L, Howells W S, 1989, J. Condens. Mat. (in press)
21. Soper A K, 1988, Proceedings of ICANS-X, held in Los Alamos, Oct 1998, to appear as IOP conference proceedings.
22. Jaynes E T, 1982, Proc. Of the IEEE, **70**, 939
23. Bryan R K and Skilling J, 1984, Monthly Not. Astr. Soc. **211**, 111
24. Lado F, 1971, J. Comput. Phys. **8**, 417
25. Throop G J and Bearman R J, 1965, J. Chem. Phys. **42**, 2408
26. Root J H, Egelstaff P A and Nickel B G, 1986, Inst. of Phys. conference series no. 81 "Neutron scattering data analysis, 1986" ed. M.W.Johnson, IOP Bristol.
27. Lighthill M J, 1959, "Introduction to Fourier analysis and generalised functions", Cambridge University Press
28. Perry G and Throop G J, 1972, J. Chem. Phys. **57**, 1827